Understanding the Effect of Panel Shape on Soccer Ball Aerodynamics using CFD

Sarmad Iftikhar

00000203341

Supervised by

Dr. Salma Sherbaz

A thesis submitted in the partial fulfillment of the requirements

For the degree of Master of Science

In

Computational Sciences & Engineering

Research Center for Modelling & Simulation (RCMS)

National University of Science & Technology (NUST)

Islamabad, Pakistan

August 2020

Statement of Originality

I hereby certify that the work embodied in this thesis is the result of original research and has not been submitted for a higher degree to any other University or Institution.

Sarmad Iftikhar

MS Computational Science & Engineering

Acknowledgements

"Rabbanaa wa la kal hamd, hamdan katheeran tayyiban mubaarakan feeh"
'Our Lord, all praise is due only to You, praise which is abundant, excellent and blessed.'
[Sahih Bukhari Vol.1, Book 12 , Hadith 764]

In the beginning, I am very grateful to the ALLAH Almighty for giving strength, good health and opportunity to complete my research work. Without His help, I would never have been able to complete this tiring task.

I would like to thank my thesis supervisor Dr. Salma Sherbaz for her constant support, guidance, mentorship and tolerance throughout the research work as well as the course work.

I would also like to express my sincere gratitude to the GEC members – Dr Rizwan Riaz (Principal RCMS), Dr Adnan Maqsood and Dr Zartasha Mustansar for their valuable suggestions and feedback.

The team members who provided me with such a cooperative and facilitating platform in the Research lab were also very crucial; for this I would thank Engr. Muhammad Usman, Engr. Muhammad Hassan, Mr Asim Younas and Mr Shahzad Khan for their assistance at Supercomputing Lab RCMS, NUST.

At the end, I would like thank to my all class fellows and lab mates: Hafiz Ali Haider, Hassan Tahir Shah, Amir Sultan, Salman ul Zaman, Faisal Asad, Haris Sohail, Hamood Ur Rahman, and Muhammad Hamza - for their support and encouragement.

Dedicated to my beloved family

Contents

List Of Tables

List Of Figures

Abstract

Football is considered as the most popular sports today and is played widely around the world. Due to increasing technological advancements and demand for better performance, the football manufacturers have been developing new designs progressively since its inception over 110 years ago. A traditional spherical football made of 32 leather panels stitched together in 1970s, has become 14 thermally bonded synthetic curved panels in 2006, 8 thermally bonded panels in 2010 and more recently 6 thermally bounded polyurethane panels in 2014 and innovative six panels design in 2018. The soccer balls having varied panels shape, number, and seam configurations have different aerodynamic behavior and flight characteristics.

Unlike other sports balls i.e. golf, cricket and tennis etc., very few research studies have attempted to examine the aerodynamics characteristics of the different soccer balls. Most of the studies conducted in the past in the area of soccer ball aerodynamics are of experimental nature and involved measurement of the forces such as drag and lift using wind tunnel testing. To the best of our knowledge, very little research has been performed on simulating the flow around different soccer balls having specific panel shape using computational fluid dynamic (CFD) techniques. The CFD analysis will allow an effective estimation of fully turbulent around the different soccer balls.

The aim of this research is to understand the effect of panel shape on soccer ball aerodynamics using computational fluid dynamics techniques. The whole study is divided into two phases. In the first phase, the turbulent air flow around a static sphere is investigated numerically for a range of Reynolds numbers using finite volume method based commercial software ANSYS® Fluent. In order to choose a suitable turbulence modeling approach, the results obtained from LES are compared with computations from BSLRSM. In the later phase, the turbulence modeling approach found adequate for predicting the complex flow field features around the smooth sphere, is used for simulating the flow around the two soccer balls (Adidas Telstar 18 and Brazuca) having six number of panels and panel shape as well as different seam

configuration. So the simulations are performed at the different incoming flow velocities ranging from 7m/s to 35m/s.

It was observed that RANS based turbulence modeling approach can be used for simulating the flow around a sphere in the laminar flow regime ($Re \leq 10^4$). However, for higher Reynolds number ($Re > 10^4$), LES is a more appropriate choice. Both Brazuca and Telstar 18 have approximately the same critical speed. Telstar 18 has a smaller drag coefficient than that of Brazuca in the narrow speed range. Nevertheless, Telstar 18 mostly has slightly larger drag coefficients. In case of Brazuca, he boundary layer separation take place around 98^o, however, in case of Telstar-18 the separation angle is around 101^o. 8. It is observed that the effect of the panel shape and seam configuration are more significant on the flow field around the soccer balls as compared to soccer ball drag coefficient.

CHAPTER 1: INTRODUCTION

1.1 Background

The football game is world's most popular, played and loved sport. The Fédération Internationale de Football Association (FIFA), being the highest governing body of football, sets the specification requirements for soccer balls used in prestigious, international soccer competitions such as the FIFA World Cup and Olympic Games. In the ensure fair and exciting matches, FIFA has devised different rules regarding equipment to be used, field of play, results settling and even the conduct of participants.

FIFA introduced its quality Programme in 1995 with the aim to standardize and improve the quality of footballs. It is a rigorous testing procedure for the soccer balls before declaring them suitable for any competitive play. It also incorporates the recent technological developments to meet the increasing demand for better performance. In order to qualify for the "FIFA Inspected" label, it is compulsory for every football to pass seven laboratory tests. Features like circumference, sphericity, rebound height, water absorption, weight, internal pressure loss and size/shape retention after prolonged use are analyzed during these tests. However, no restrictions have imposed on the surface design/geometry of the soccer ball due to which the football manufacturers have been developing new designs progressively since its inception over 110 years ago [1}.

Figure 1.1. Evolution of the soccer ball since 1930 [1]

Adidas Telstar used for the 1970 Mexico World Cup Finals had 32 panels (20 hexagonal and 12 pentagonal panels). In order to enhance the performance characteristics of Adidas Telstar, during 2002 World Cup, a refined syntactic foam layer was added to it. The conventional 32 panel design was replaced by 14 thermally bounded curved panels Teamgeist used in 2006 World cup. Adidas Jabulani was the official match ball for the 2010 FIFA World Cup. It consisted of 8 thermally bounded panels and a textured surface to improve its aerodynamic performance. Adidas Brazuca and Telstar 18 were the match balls for the 2018 and 2014 World Cups, respectively. Both of these balls have same panel number (six thermally bonded textured panel) but totally different panel shapes.

1.2 Surface Structure Effect on Soccer Ball's Aerodynamics

The soccer balls having varied panels shape, number, and seam configurations have different aerodynamic behavior and the flight characteristics [2-7]. For example, the total seam length of Brazuca was 68% more than that of Jabulani's. Due to increase in the seam length the total surface roughness of the ball was also increased. This helped in pushing its drag crises to a lower Reynolds number than Jabulani while keeping the drag coefficient constant during the speed ranges common for corner and free kicks [8].

1.3 Research Objectives

The aim of this research is to understand the effect of panel shape on soccer ball aerodynamics using computational fluid dynamics techniques. Following objectives have been set to achieve this aim

1. Simulate the flow field around a smooth sphere having same dimensions as that of soccer balls under consideration (Adidas Brazuca and Telstar 18) using unsteady RANS (URANS) and LES.
2. Selection of an appropriate turbulence approach for calculation of turbulent flow around spherical objects.
3. Simulating the turbulent flow over the two soccer balls Adidas Brazuca and Telstar 18 using a suitable turbulence modeling approach.

The main reason for choosing Adidas Brazuca and Telstar 18 for the current study is the fact that both of these balls have the same number of panels.

1.4 Research Methodology

In order to investigate the understand the effect of panel shape on soccer ball aerodynamics, the whole study is divided into two phases. In the first phase, the turbulent air flow around a static sphere is investigated numerically for a range of Reynolds numbers using finite volume method based commercial software ANSYS® Fluent. In order to choose a suitable turbulence modeling approach, the results obtained from LES are compared with computations from BSLRSM.

In the later phase, the turbulence modeling approach found adequate for predicting the complex flow field features around the smooth sphere, is used for simulating the flow around the two soccer balls having varied number of panels and panel shape as well as different seam configuration. The effect of panel shape on soccer ball aerodynamics is analyzed. The overall research methodology implemented in the current research is also illustrates in Figure 1.2.

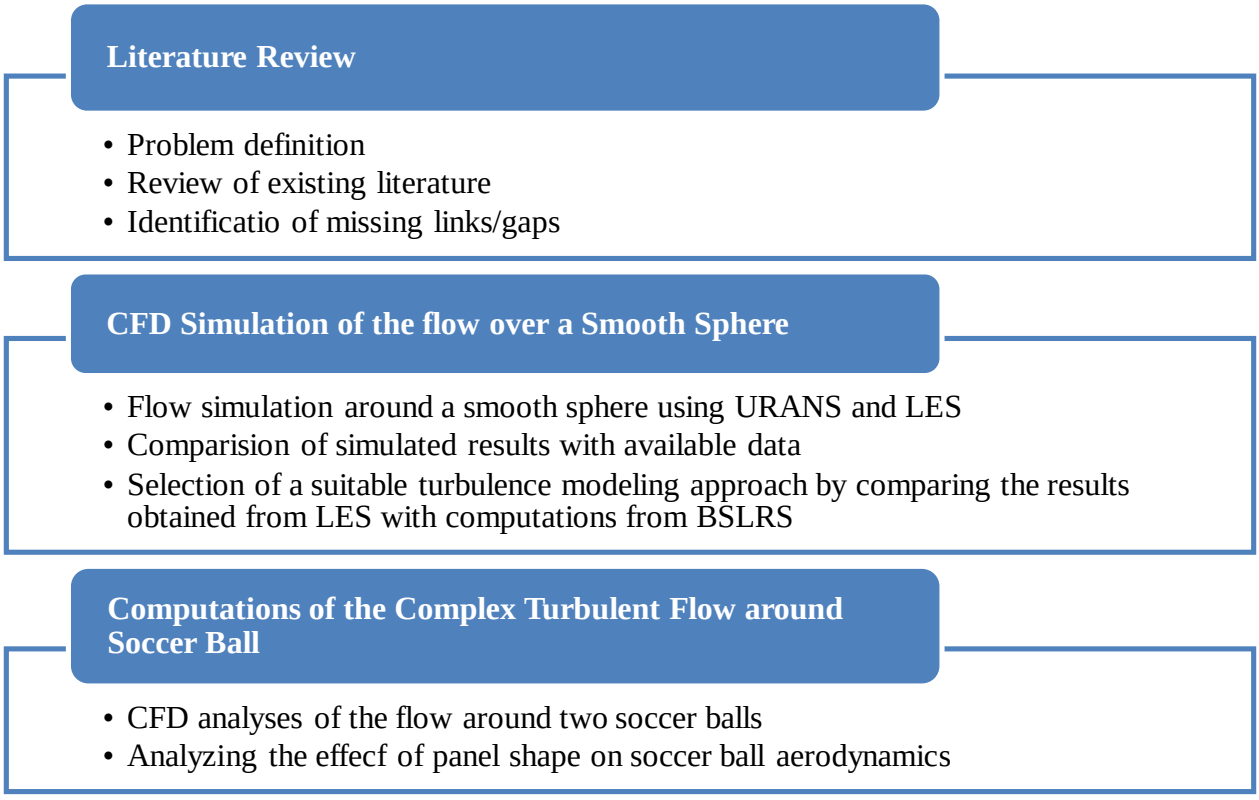

Figure 1.2. Research methodology

1.5 Contributions

Although, flow around the different soccer balls have been extensively studied using experimental techniques. A very few studies examined the aerodynamic behavior of the different soccer balls having varied number of panels and seam configurations using Computational Fluid Dynamic (CFD) techniques.

1.6 Relevance to National needs

Sports goods industry of Pakistan has a reputable standing in the international market for its superior quality sports goods. During the year 2015-16, the share of Pakistan sports goods was around 1.51% in the total exports with football as major export product having 43% share of total sports goods exported in 2012-13[9]. Various famous global brands like Nike, Puma, Adidas, Decathion, Select, Litto, etc. have their soccer balls produced in Sialkot.

The research focused on the aerodynamic study of the different soccer balls using computational fluid dynamic techniques will pave the path for future research in the area of sports aerodynamics.

1.7 Organization of the Thesis

Chapter 1 --- Introduction

This chapter provides a brief summary of the historical evolution of the soccer ball surface geometry with respect to the shape, number, and orientation of their panels. The underlying objectives of the current research and adopted research methodology adopted is also outlined.

Chapter 2 --- Literature Review

This chapter provides a brief overview of the research in the area of soccer aerodynamics.

Chapter 3---Methodology

This chapter provides a comprehensive overview of the mathematical models and computational setup used in this research project.

Chapter 4 --- Results and Discussion

This chapter includes a discussion of the main findings from the research.

Chapter 5 --- Conclusions and Future Work

The summary of important conclusions derived from the current research are presented. Recommendations for future efforts in this area are also suggested in this chapter.

CHAPTER 2: LITERATURE REVIEW

The previous research conducted on the aerodynamics of the soccer balls can be divided into two broad categories. The first category includes the studies that measures the aerodynamic properties of the different soccer balls using wind tunnel testing and computational fluid dynamics techniques. The second category deals with the research related to the soccer ball trajectory analysis. An overview of the different research studies under these categories is given in the following paragraphs.

2.1 Measurement of Soccer Ball's Aerodynamic Properties

2.1.1 State of Experimental Work

The previous studies in the area of soccer ball aerodynamics, mostly involved wind tunnel testing. M. J. Carré et. al. [10] used the wind tunnel measurements for soccer ball to study the effect of boundary layer transition from laminar to turbulent behavior on the drag coefficient at high Reynolds number. For spinning soccer balls, the reverse Magnus effects were observed at low Reynolds numbers (as shown in Figure 2.1). The seams on the soccer ball surface also resulted in a more predictable Magnus behavior.

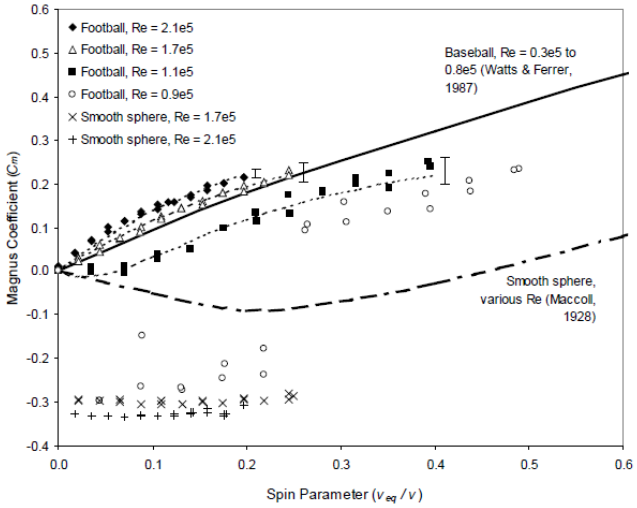

Figure 2.1 Magnus coefficient for spinning balls over a range of velocities [10].

T. Asai et.al. [11, 12] performed the wind tunnel experimentation to compare the aerodynamic coefficients of the static and rotating soccer balls. A titanium tetrachloride visualization method was also used to study the vortex dynamics of soccer balls in flight. During the visualization experiments it was observed that the boundary-layer separation point for a non-rotating ball was around 90° during a low-speed kick (5 m/s), and receded to approximately 120° during a high-speed kick (29 m/s).

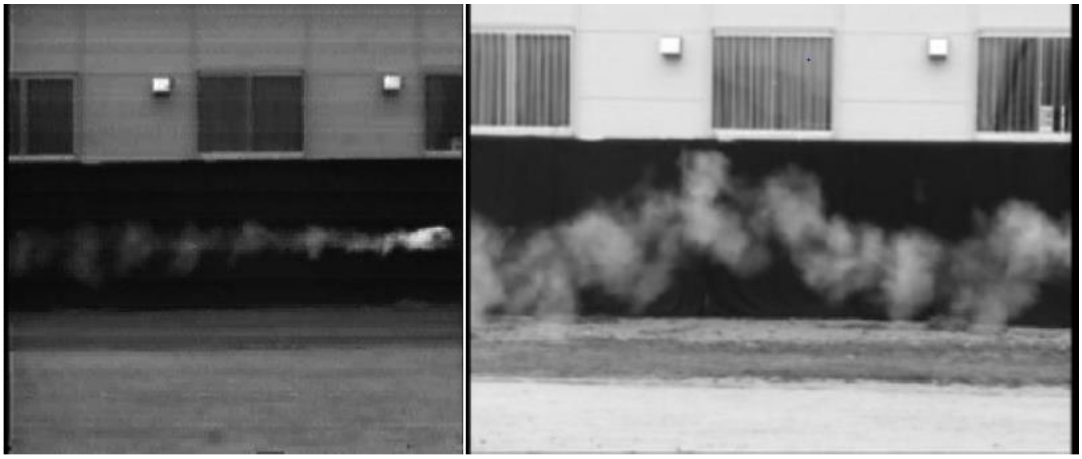

Figure 2.2 Wide-angle view of the vortex pathway for a non-rotating ball [11, 12]

The aim of the experimental study conducted by L. Oggiano, and L. Sætran [13] was to measure the drag and side forces of the different soccer balls in the static and spinning conditions. By implementing the experimental data in a Matlab routine, the free kick simulations were performed. It was concluded that the panel shapes, panel number, surface dimples and different seaming have a substantial effect on the the flight trajectories of the different soccer balls (shown in Figure 2.3).

M. Passmore, et.al. [14] Conducted the wind tunnel testing to measure important factors including Reynolds sensitivity effects, Magnus effects, and low spin rate orientation (knuckle) effects and unsteady aerodynamic loads of the several FIFA approved footballs. It was concluded that the different drag characteristics and unsteady aerodynamic loads of these soccer balls had a limited effect on their unpredictable flight behavior. However, significant differences in the lateral aerodynamic forces for these balls resulted in different flight path in both spinning and slowly rotating conditions.

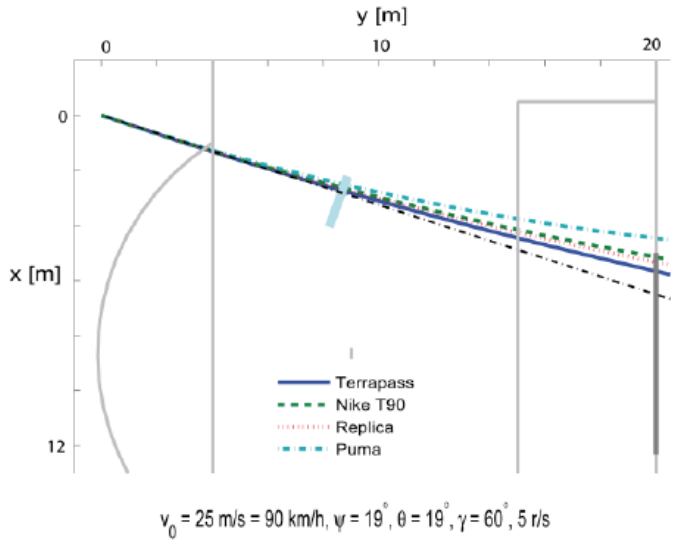

Figure 2.3. Simulated trajectories of the four different soccer balls [13]

The purpose of the experimental study conducted by T. Asai et. al. [15] was to compare the basic aerodynamic characteristics of an 8-panel soccer ball (Adidas Tango 12) with those of a new 32-panel soccer ball (for Euro 2012). It was observed that critical Reynolds number (3.3×10^5) for 8-panel ball was slightly higher than that of new ball (2.4×10^5). Similarly, the drag coefficient of the new 32-panel ball was found much closer to that of a golf ball than an 8-panel soccer ball (as shown in Figure 2.4).

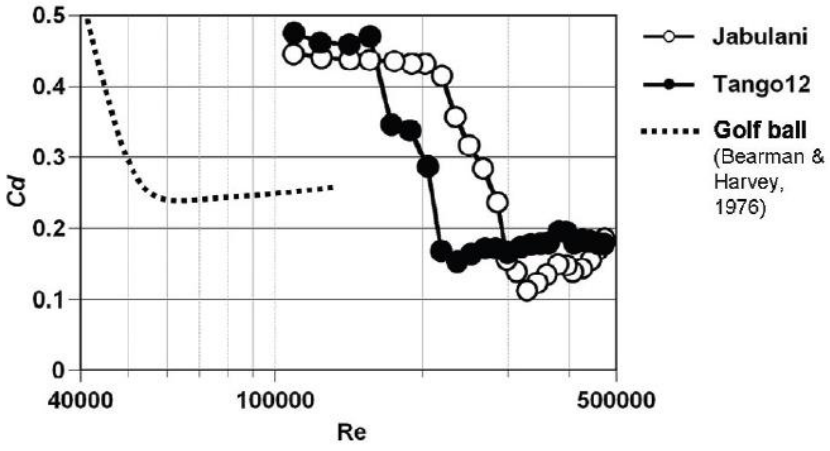

Figure. 2.4. Drag coefficient versus Reynolds number curves for 8-panel ball (Jabulani) and new ball (Tango 12) [15]

T. Asai and K. Seo [16] performed a steady state analysis of the four different soccer balls with varied number of panels i.e. Adidas Tango 12, Adidas Roteiro, Adidas Teamgeist II, and Adidas Jabulani having 32, 32, 14 and 8 panels respectively. The parameters recorded during these experiments include drag coefficient and critical Reynolds numbers. The effect of the drag coefficient on the flight trajectory and ranges was analyzed with the help of simple 2D flight trajectory simulation. A strong correlation was found between the critical Reynolds number and the total seam length on the soccer balls.

F. Alam et. al. [17-20] experimentally evaluated the aerodynamic forces and moments for several FIFA-approved soccer balls over a range of wind speeds. The non-dimensional drag coefficients were also calculated and compared. In a similar experimental study performed by F. Alam et. al. [6], the effects of surface structure on the aerodynamics performance of six different soccer ball was evaluated. It was reported that surface structure has a significant effect on the flow regime around different balls and their drag coefficients.

S. Hong et.al. [22], presented the results of their experimental study in which the trajectory and aerodynamic characteristics of the four different soccer balls having varied panel number and panel shape, were examined. The experimental results indicated that panels number and their orientation has a significant effect on the aerodynamic forces. Similarly, the panel shape and orientation were more important as far as the flight trajectory of the soccer balls was concerned.

J. E. Goff et.al. [8] reported the results of wind tunnel measurement of the drag coefficient for non-spinning Jabulani and Brazuca balls. The critical drag speed of Brazuca was found lower and super-critical drag coefficient was higher than that of Jabulani. The drag data was also used in simulating the trajectories of these soccer balls.

S. Hong and T. Asai [7] studied the effect of surface dimples on the aerodynamic characteristics of the 10 different soccer balls and confirmed that existence of dimples on the ball surface had a considerable effect on the aerodynamic forces. In a similar experimental study performed more recently by S. Hong et.al [25], the aerodynamics of the five different soccer balls (each having 32 panels with different surface structures) were examined via wind-tunnel experiments.

2.1.2 State of Computational Work

M. J. Carré et.al. [26] analyzed the effect of incoming flow velocity and spin conditions on the aerodynamic properties of a generic soccer ball using wind tunnel testing and computational fluid dynamics. S. Barber et.al. [27] used CFD to evaluate the effect of seam width and sharpness on the ball's aerodynamic behavior. In another numerical study performed by S. Barber et.al. [28], the Reynolds Averaged Navier–Stokes approach with the realizable k-ε turbulence model was used to calculate the drag, lift and side force coefficients as well as the pressure distributions near the stagnation point.

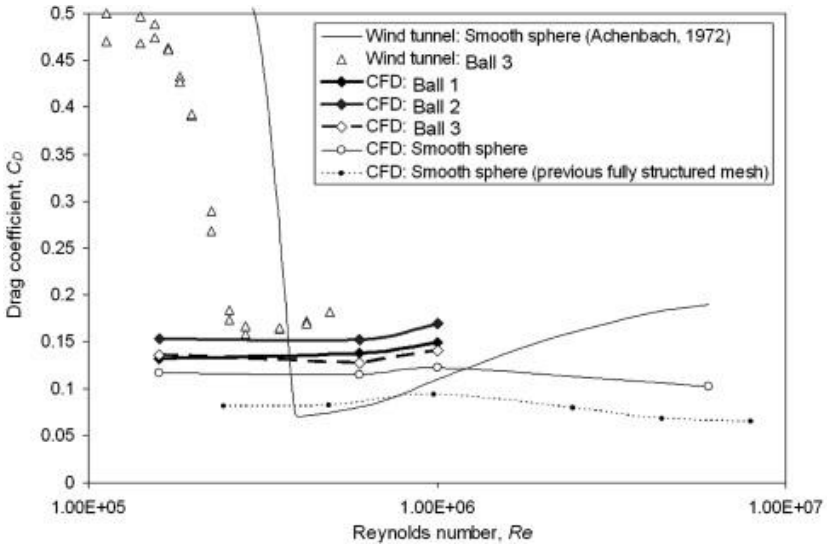

Figure 2.5. Drag Coefficient vs. Reynolds Number for three soccer ball and a Smooth Sphere [27]

P. Jalilian et. al. [29] used computational fluid dynamics to analyze the effects of spin rate and surface pattern on the aerodynamic forces acting on different sports ball (baseball, volleyball and two soccer balls). A strong correlation was observed between ball spin rate and the drag and lift forces acting on these balls.

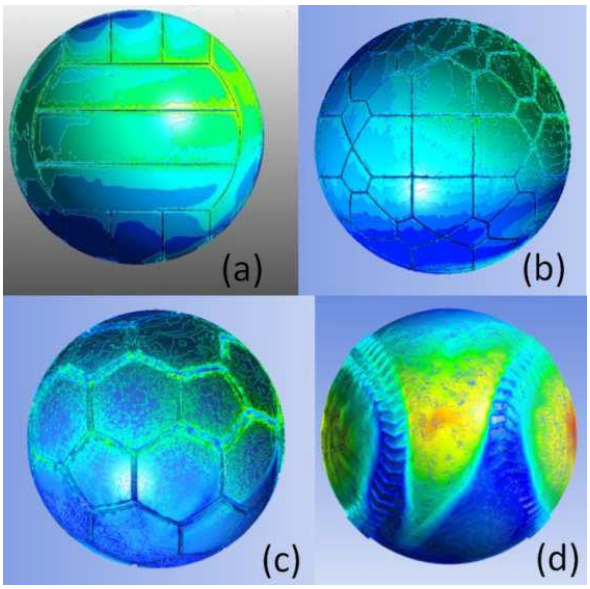

Figure 2.5. The surface shear stress distributions for (a) volleyball, (b) the 86-panel soccer ball, (c) the generic soccer ball and (d) baseball [29].

Rohr [30] calculated the aerodynamic effects of the seam on a two-dimensional representation of a non-rotating soccer ball using CFD. The effects of the seam on the boundary layer and overall transient flow structure was modeled using a transitional solver. The author reported a local effect of the seam on the skin friction however this effect was not strong enough to delay the separation point as predicted by previous literature. S. B. Hussain et. al. [31] performed a numerical study of a smooth sphere and a 32-panel conventional soccer ball to analyze the effects of surface geometry on the aerodynamic characteristics of the soccer ball. K-epsilon turbulence model was used. The calculated results were compared with available numerical [28] and experimental results.

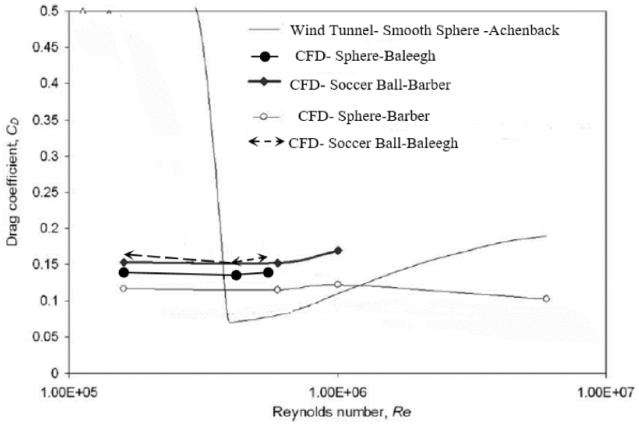

Figure 2.5. Comparison between the calculated and available results [28]

T. Asai et.al. [32] used lattice Boltzmann method, wind tunnel testing and free-flight experiments to investigate the aerodynamic characteristics and flow field around a soccer ball. It was concluded that the trajectory of the spinning ball is stable and regular even after the deflection due to the shifting of the boundary layer separation points.

2.2 Trajectory Analysis

Trajectory analysis is a method for studying soccer balls in environments more representative of game play than those provided by wind tunnels [33-36]. Such analyses mostly require a ball launcher and optical or radar-based sensors for measuring the spatial co-ordinates of the trajectory [37, 38]. Although the wind tunnel testing is a natural choice for studying the aerodynamics of different soccer balls. During a wind tunnel test, air is moved across a ball while sensors measure the magnitude and direction of force. The calculation of the aerodynamic characteristics using trajectory analysis has several advantages over the wind tunnel experimentation e.g. it eliminates the use of a support rod which may affect aerodynamic studies in wind tunnels, and can calculate lift coefficients in regions inaccessible by many wind tunnels [34].

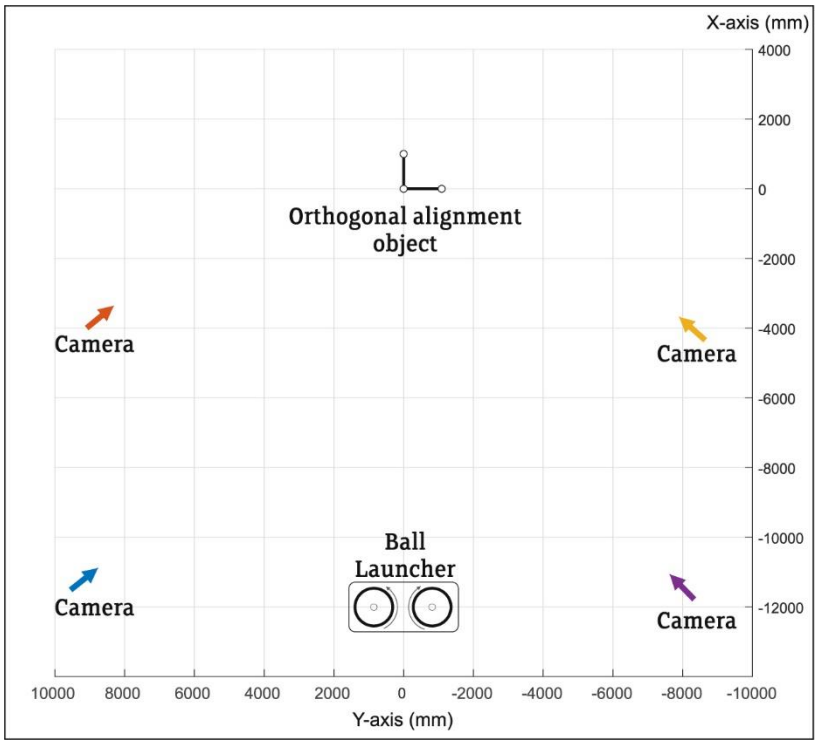

Figure 2.6. Trajectory analysis setup example [36]

Researchers have used trajectory analysis to study the dominant interactions between ball and air [39]. The information related to boundary layer separation can also be extracted using this method [40]. The two most important kicks in the football game i.e. a direct free kick and a corner kick can be modelled using this technique [33, 41]. More recently, wind-tunnel experimentation and trajectory analysis were combined to show the increased aerodynamic stability of the Brazuca (used in the 2014 World Cup) over the Jabulani (used in the 2010 World Cup) [8].

2.3 Missing Links in Literature and Purpose of this Work

The previous studies in the area of soccer ball aerodynamics, mostly involved measurement of the forces such as drag and lift using wind tunnel testing. A few studies examined the aerodynamic behavior of the different soccer balls having varied number of panels and seam configurations using Computational Fluid Dynamic (CFD) techniques. A detailed CFD analysis is required for effective comparative estimation of fully turbulent around the different soccer balls.

The aim of this study to fill the gap in the previous computational research by the precisely modelling the effects of the panel shape on a soccer ball aerodynamics using CFD. For this purpose, two different turbulence modeling approaches were used i.e. RANS BSLRSM and LES. The effect of different panel shape on the boundary layer separation point, and overall wake structure are observed. This study, in tandem with experimental work, will creates a well-rounded analysis of the effects of panel shape on soccer ball aerodynamics.

CHAPTER 3: METHODOLOGY

In this chapter, a detailed overview of the computational setup used in this research project is described. It includes a systematic explanation of each step carried out in the CFD analysis from geometry modeling, grid generation, selection of appropriate turbulence model, flow parameters, boundary conditions, solver setting to convergence criteria. To check the validity of the computational setup, experimental results will be compared with the numerical results obtained in CFD analysis.

The use of Computational Fluid Dynamics (CFD) techniques to simulate the flow around geometrically complex shapes such as airplanes, cars, ships, and combustor has become a common engineering practice since last few decades. Computational Fluid Dynamics being a very powerful tool, is used in design engineering, optimization, structure analysis and many other applications. A number of available general purpose CFD codes like OpenFoam, Fluent, CFX, X-FLOW, COMSOL and STAR-CCM+, etc. can be used to perform such studies. The availability of an excellent preprocessing software component is considered as a strength of any CFD code. It allows robust meshes to be constructed around very complicated shapes, and the number of quite advanced turbulence models contained within them. Whilst these codes are now also developing the ability to handle problems with moving and deforming meshes, these features are typically structured around particular geometries of commercial importance, such as piston motion in cylinder blocks, fan blades in cyclones and stores separation from aircraft.

In this report we have simulated the flow around a smooth sphere and two different soccer balls using the finite volume method-based code ANSYS® Fluent over a range of Reynolds numbers (Re). The purpose was to cover the different flow regimes, varying from laminar steady-state flow near Re = 100 to turbulent flow at $\mathrm{Re} = 10^6$.

3.1 Theoretical Background

Computational Fluid Dynamics (CFD) refers to the use of different numerical techniques to give the approximate solution of governing equations of fluid flow. As mentioned earlier,

commercially available software ANSYS® Fluent is employed as the computational solver in this study. The equations governing the current fluid flow problem are explained initially followed by the details of the available turbulence models and reasoning for the selection used for this study. Finally, a detailed explanation of the overall framework for the solution process provided.

3.1.1 Governing Equations

The fundamental governing equation of fluid dynamics i.e. Continuity, Momentum, and Energy equations are based on the universal laws of conservation of mass, momentum and energy respectively. The detailed derivation of these equations can be found in [43] In the present research, three-dimensional flow of a viscous, incompressible fluid is considered. The resulting governing equation i.e. continuity and momentum take shape

1. Continuity: $\boldsymbol{\nabla} * \boldsymbol{V} = 0$

2. Momentum: $\rho \frac{\partial V}{\partial t} = \rho \boldsymbol{f} - \boldsymbol{\nabla} p + \mu \nabla^2 \boldsymbol{V}$

Where ρ and $\boldsymbol{V}$ are the fluid density and velocity respectively. Whereas $\boldsymbol{f}$ is body force, and μ is the coefficient of dynamic viscosity. The above two equations along with the energy equation are mostly referred as Naiver Stokes (NS) equations. A turbulence model is required to numerically solve the governing unsteady NS equations for any turbulent flow problem.

3.1.2 Turbulence Model

The most accurate approach for simulating turbulent flows is called the direct numerical simulation (DNS). This method is devoted to find the direct solution of the unsteady NS equations and does not need any additional closure equations. As the DNS method resolves even the smallest eddies and time scales of turbulence within a flow domain, extremely small time steps and very fine grids are required to find accurate solutions. Due to these restrictions, DNS method is mostly applied to low Reynolds number flows and small-size computation domains. Therefore, DNS will not be used to simulate the current high Reynolds-number complex flow [43-46].

Another option is the use of Large-eddy simulation (LES) solvers which accurately predicts the large scale turbulent structures within the flow domain and uses subgrid scale model to

represent the smaller scale eddies. This results in a major reduction in the computational cost compared to DNS. Though LES only resolves the large scale eddies, an extremely fine grid is still required to resolve energy-containing eddies. This method has been successfully used for solving numerous high Reynolds number flow problems [47, 48]

In some cases, one might not need the detailed instantaneous flow simulations and only be interested in the steady-state fluid flow. This approach leads to a profound reduction in the computational time and forms the basis for the Reynolds-averaged Navier–Stokes (RANS) technique. In RANS approach, only the averaged quantities are solved and a suitable turbulence model is used to capture all the scales of instantaneous turbulent motion. Owing to the modest computing requirement of RANS based solvers, they have been widely used in the industrial CFD applications. However, in many cases where the information regarding the transient flow behavior is required, RANS approach is not sufficient.

In RANS approach, the time averaged terms in continuity and momentum equations are written with bars as shown below [50]:

1. **Continuity:** $\frac{\partial \bar{u}_j}{\partial x_j} = 0$,
2. **Momentum:** $\frac{\partial}{\partial t}(\rho \bar{u}_i) + \frac{\partial}{\partial x_j}(\rho \overline{u_i u_j}) = -\frac{\partial \bar{p}}{\partial x_i} + \frac{\partial}{\partial x_j}(\bar{\tau}_{ij} - \rho \overline{u'_i u'_j})$,

Where as $\bar{\tau}_{ij}$ has the reduced form: $\bar{\tau}_{ij} = \mu \left(\frac{\partial \bar{u}_i}{\partial x_j} + \frac{\partial \bar{u}_j}{\partial x_i}\right)$, i,j,k=1,2,3. Similarly, u_1, u_2, u_3 are the components of velocity in x, y and z direction respectively. The additional term $-\rho \overline{u'_i u'_j}$ in the momentum equation is called Reynolds stress. For any turbulent flow simulation, a turbulence model is required to compute the Reynolds stress with a reasonable accuracy.

Different turbulence models available in literature can be divided into two broad categories, i.e. Eddy Viscosity Models (EVM) and Reynolds Stress Models (RSM).

The EVM use the Boussinesq assumption and considers a functional relationship between the Reynolds stress and the strain rate. The various categories of EVMs can be found including algebraic or zero equation, one and two equations models. Baldwin-Lomaxmodel [51] is an example of zero equation model which calculates the eddy viscosity as a function of mean flow quantities. Due to the strong reliance of these models on the boundary layer flow assumption, they are not considered sufficiently accurate. Similarly, several one equation

EVMs have been developed in the past. These models use a single transport equation to determine the eddy viscosity. Spalart-Allmaras Model is an example of one such models. Two equation turbulence models used to transport equations to account for the turbulent flow characteristics. The k-epsilon and the k-omega model are the examples of famous two equation models commonly used for different types of industrial flow problems. However, the active research in the area of two equation EVMs is still going and new refined models are still being developed [52].

On the other hand, in RSM, a more sophisticated approach is adopted by calculating the solution of seven transport equations, one for each of the Reynolds stresses themselves, and an additional equation to obtain the length scale of the local turbulence. In the complex flows problems involving the high degrees of anisotropy, flow separation and re-circulation zones, the RSM approach is usually required [53].

3.1.3 Selection of a suitable Turbulence Model

As mentioned in the previous chapter, most numerical investigations found in literature, on fluid flow around the different soccer ball have been focused on using steady state RANS solver. Most of these studies were unable to capture the drag crisis characteristics at $10^5 < Re < 10^6$. So in order to choose a suitable turbulence model for flow simulation around a soccer ball, the whole study in two phases. In the first phase, the flow around a sphere was simulated using both unsteady RANS solver and LES approach. After the selection of most suitable turbulence modeling approach for a sphere, the same approach was used for soccer ball simulations in the second phase of the study.

Z.Q. Leong [54] et al. simulated the flow around smooth sphere to examine the performance of RANS-based solver with and without turbulence models. The turbulence models considered for this study were Shear Stress Transport k-omega (SST) and Baseline Reynolds Stress Model (BSLRSM). The simulations were carried out at different Reynolds number ranging from 10^2 to 10^6. The calculated values of mean drag coefficient (C_D) were compared with the experimental results by Schlichting [55]. It was observed that in the fully turbulent flow regime (at $Re = 10^6$), the agreement between BSLRSM predictions and experiment results was much closer than that of SST model.

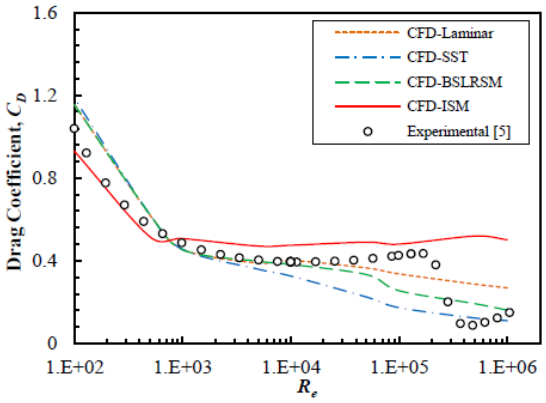

Figure 3.1: Comparison between the calculated values of drag coefficient of the sphere with the experimental results [54]

Similarly, D.A. Jones and D.B. Clarke simulated the various flow regimes around a smooth sphere [56]. For $20 < Re < 200$, the flow is steady-state and axisymmetric, whereas at Re=300 the flow becomes unsteady and shows a periodic time-dependent behavior. Similarly, at Re = 10^4, the boundary layer flow still remains laminar but the flow in the wake becomes turbulent. Whereas at a Reynolds number of approximately Re = 3.8 ×10^5 the boundary layer switches from being predominantly laminar to predominantly turbulent, hence the separation point moves further downstream, the wake narrows, and the drag coefficient drops considerably (A summary of the different flow regimes around a sphere is also presented in Table 3.1). To simulate the first two cases, the laminar calculations were performed. LES simulation using the Dynamic Smagorinsky sub-grid scale model with a fine mesh were performed for the last two Reynolds numbers.

Table 3.1: Different flow regimes around a sphere [56]

Re range	Nature of Flow	Drag coefficient	Strouhal number
$20 \leq Re \leq 210$	Steady axisymmetric flow with closed recirculating wake in the shape of a vortex ring.	$2.7 \rightarrow 0.7$	Steady state flow
$210 \leq Re \leq 270$	Flow is attached, stable and consists of two streamwise vortical tails of equal strength and opposite sign. Flow exhibits planar symmetry.	C_d continues to fall monotonically	Steady state flow
$270 \leq Re \leq 300$	Transition to unsteady wake consisting of the periodic shedding of a series of interconnected vortex loops. Flow still exhibits planar symmetry.	Mean value of $C_d \approx 0.66 - 0.68$	$S_t \approx 0.14$
$400 \leq Re \leq 800$	Vortex loops continue to be shed but the azimuthal angle at which they are formed begins to oscillate in an irregular fashion and the planar symmetry is lost.	Mean value falls to 0.5 at Re = 800	S_t slowly increases to 0.2 at Re = 800
$800 \leq Re \leq 3.8 \times 10^5$	Vortex loops continue to be shed but in a more irregular manner, although strong periodic fluctuations still exist in the wake.	$C_d \approx 0.5$ over entire range	$S_t \approx 0.2$ over entire range
$3.8 \times 10^5 \leq Re \leq 1.14 \times 10^6$	Near wake region shrinks considerably, drag decreases sharply, periodic vortex shedding is no longer able to be detected experimentally.	$C_d \approx 0.08$ at the critical point, then slowly rises to ≈ 0.12	Considerable uncertainty exists in the literature

Following the results reported in above two research studies, the flow around a smooth sphere (having the same dimensions as that of the soccer balls) is first simulated using BSLRSM and LES models. The calculated results in both cases are compared with available experimental results. A model capturing the drag crises characteristics successfully is further used in simulating the flow around the soccer balls.

3.2 CFD Framework

A systematic procedure was followed to develop a suitable computational setup. There are mainly three stages involved in CFD analysis i.e. pre-processing, processing and post-processing. A brief introduction to each of them is given in the following paragraphs

In pre-processing stage, formulation of flow problem is carried out through an intensive and continuous brainstorming process. Formulation of flow problem answers some basic "Wh" questions like, why one is performing this analysis? What is the objective of the analysis? What is the nature of the problem? Is it a 2D problem or 3D? Is it a steady case or unsteady? Is the flow compressible or incompressible? Is it a laminar or turbulent flow problem?

Formulation of flow problem is followed by the generation of geometry and creation of the flow domain. In creating the flow domain, the shape, size, and upstream-downstream extents

of the domain are figured out. In the proceeding steps flow domain is discretized into an appropriate number of points, typically known as a grid/mesh generation process. Flow parameters are inserted into the solver and a suitable turbulence model is chosen (if needed). Boundary and initial conditions are set up. Reference values needed to calculate certain flow parameters are given to the solver. Finally, a convergence criterion is defined in terms of residuals.

Processing refers to that course of the CFD analysis in which a simulation is running on the system and the discretized algebraic equations are being solved up by the computer in the form of matrices. Although processing stage of the analysis mainly involves a computer system, sometimes a human is needed to keep track of the residuals so that he could make necessary changes in case the solution diverges or encounters any other issue.

In the post-processing stage of the CFD analysis, desired results are extracted by the user of the CFD code. These results could be in the form of tables, graph plots, colorful diagrams (contours) and/or flow animations, etc. The typical steps involved in a CFD analysis are shown in Figure 3.2.

The development of computational setup for flow analysis over the Smooth sphere and soccer balls will be discussed in the following paragraphs.

Since the current research is expected to lay down a basic methodology on which further research can be expanded upon, both numerically and experimentally. This section serves as an architectural framework of the overall solution process used in this study. First of all, the model geometry creation will be explained. The grid generation process and the solver settings will be discussed in subsequent sections.

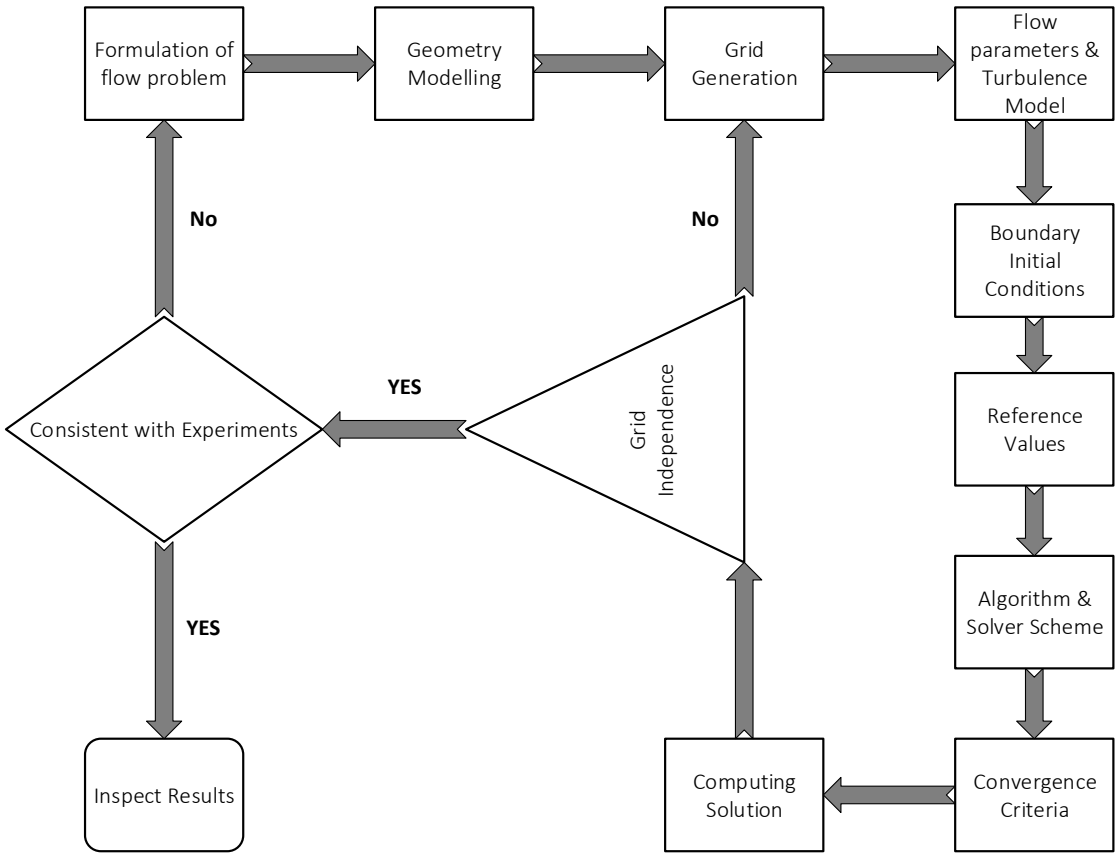

Figure 3.2 CFD process flow chart

3.2.1 Model Geometry

Two different soccer balls (Adidas Brazuca and Adidas Telstar18), each having a diameter of 220mm and a smooth sphere having the same dimensions, are used in the current study. Adidas Brazuca was the official match ball of 2014 FIFA world cup. Similarly, Telstar18 was used in FIFA world cup 2018. Both Brazuca and Telstar have six thermally bonded panel. The others important parameters like seam length, width and seam heights for both balls are summarized in Table 3.2 [57].

(a) (b)

Figure 3.3 (a) Adidas Brazuca and (b) Telstar 18 soccer ball [57]

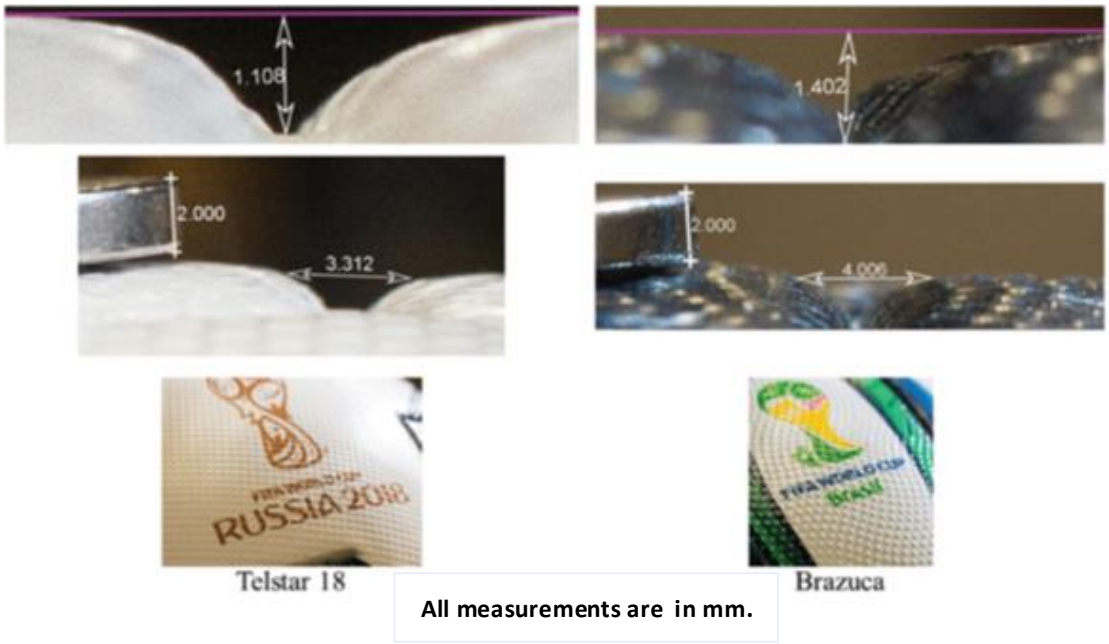

Figure 3.4. Geometric specifications of the two soccer balls [57]

Table 3.2. Geometric details of Adidas Brazuca and Telstar 18 [57]

Soccer Ball	Overall Seam Length (mm)	Seam Height (mm)	Seam Width (mm)
Brazuca	3270	1.402	4.0
AdidasTelstar18	4320	1.1	3.312

In order to create realistic soccer ball geometry, the CT scan facility available at Quaid-e - Azam International Hospital, near H-13, Islamabad was utilized. The resolution was set to 1mm. Mimics Innovation Suite was used to generate the 3D model of Telstar18 soccer ball using CT scan files. However, the geometric details of 3D Telstar18 soccer ball generated from this process were not sufficient. So the 3D models of the both soccer balls were created using SpaceClaim modeler available in ANSYS® software. The seam details given in the Table 3.2 were used during the geometry creation process.

(a)

(b)

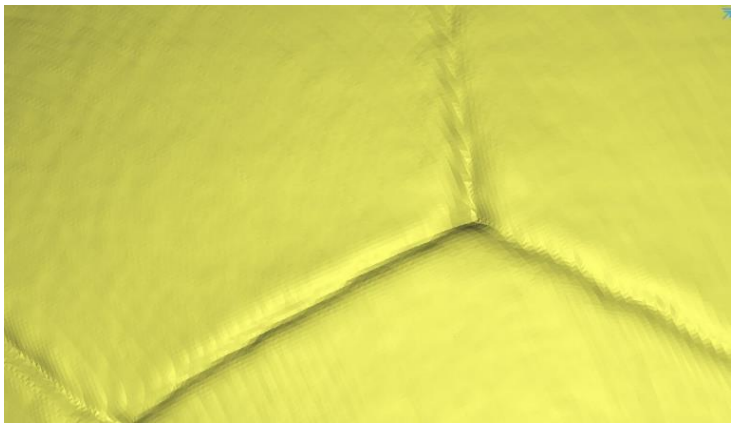

(c)

Figure 3.5. (a) CT Scanner, (b). 3D model of Telstar18 soccer ball using CT scan files, (c). Zoomed in view of soccer ball surface

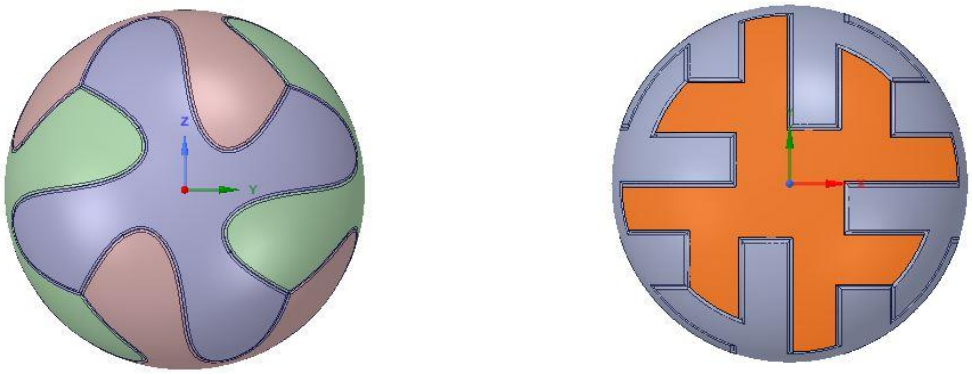

Figure 3.6. 3D models of the both soccer balls created using SpaceClaim

3.2.2 Computational Domain, Grid Generation

The computational domain around all models' sphere/balls is of rectangular shape with inlet and outlet boundaries located at a distance of 5D and 10D respectively (D is the diameter of sphere/balls). Similarly, bottom and sides of the domain are located at a distance of 5D from the balls/sphere surface.

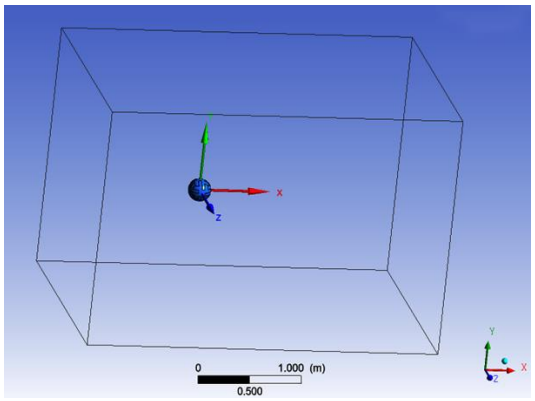

Figure3.7. Computational domain around soccer ball

The process of dividing the domain of interest into several small portions/chunks is termed as grid/mesh generation. High quality, appropriate grid generation is considered one of the key factors to obtain accurate CFD results. Simulation time, stability and convergence of the solution are also affected by the quality and type of the mesh used. Mesh generation is usually considered the most time taking process in a CFD analysis. A triangular mesh was generated

using ANSYS ICEM CFD® software. The triangular mesh has the capability of accurately capturing shape of the model of interest. Triangular meshing is generally used when the geometry is very complex. In order to capture the boundary layer separation more accurately, ten prism layers were created along the normal-wall direction starting from the balls/sphere surfaces. The height of the first cell in prism layer was taken as 0.07mm. LES requires mesh and time-step sizes sufficiently fine to resolve the energy-containing eddies. The mesh resolution governs the fraction of the energy spectrum directly resolved. In the present study, our goal was to have a mesh fine enough so that it will resolves 80% of the turbulent kinetic energy.

The velocity inlet and pressure outlet boundary condition were prescribed at the inlet and outlet boundaries respectively. Non-slip wall condition was imposed at the ball/sphere surfaces and free slip condition at all sidewall boundaries.

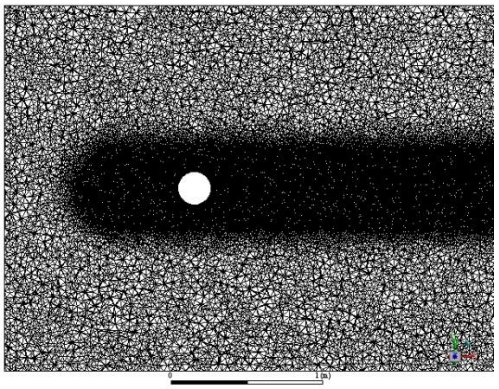

(a)

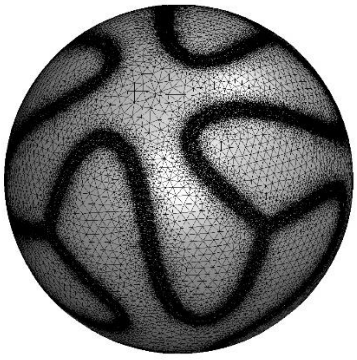

(b)

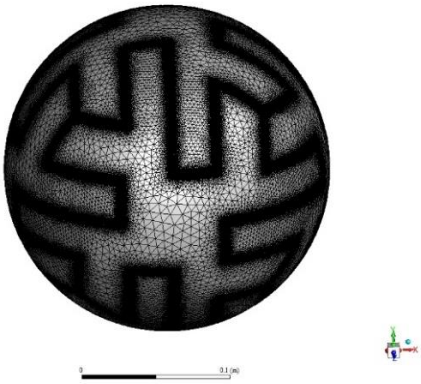

(c)

Figure 3.8. (a) Mesh around smooth sphere (b) Zoomed in view of the mesh on the Brazuca surface (b) Zoomed in view of the mesh on the Telstar-18 surface

3.2.3 Boundary Conditions

Velocity-Inlet boundary condition is used to define the flow velocity at inlet boundary. The inlet turbulence intensity as 1. 5% and turbulent length scale as 0.0154m were also specified. Whereas pressure-outlet, with gauge pressure of 0 Pascal and turbulence properties identical to those at inlet boundary were imposed at the domain outlet boundary.

3.2.4 Solver Settings

A Fluent fluid flow analysis system was created in ANSYS® workbench for the purpose of seamless project flow. Three-dimensional, incompressible transient flow simulations are performed. The wall-adapting local eddy viscosity (WALE) model is used for sub grid-scale turbulence modeling. Pressure based solver with implicit time integration is employed. The coupled algorithm is used for pressure velocity coupling. Second order scheme is used for the discretization of pressure and momentum equation. Bounded second order scheme is used for temporal discretization. The residual history is monitored to examine the iterative convergence. The simulations are performed on RCMS super computer, available at Super-Computing Research and Education Center (ScREC), RCMS, NUST.

CHAPTER 4: RESULTS AND DISCUSSION

A series of simulations are conducted to analyze the effect of the panel shape on soccer ball aerodynamics using following steps

1. First the flow around the smooth sphere (having the same dimension as that of soccer balls) is simulated using two different turbulence modeling approaches. The numerically computed values of drag coefficient and pressure distribution around the sphere are validated with available results.

2. Selection of an appropriate turbulence approach for calculation of turbulent flow around spherical objects.

3. Simulating the turbulent flow over the two soccer balls (Adidas Brazuca and Telstar 18) using turbulence modeling approach selected in the previous step.

4. Analyzing the effect of panel shape on soccer ball aerodynamics.

This chapter provides a discussion of the main findings from the research.

4.1 Flow Simulation around a Smooth Sphere

First, the flow over a smooth sphere having the same dimension as that of a soccer balls (Adidas Brazuca and Telstar 18) is simulated to select an appropriate turbulence model approach, validate meshing strategy, boundary conditions and solution methodologies. The available experimental/numerical data for the flow over a smooth sphere at the same flow conditions is used for the validation purposes [58-59]. Transient simulations are performed at an over a range of Reynolds numbers (Re) to cover the different flow regimes, varying from laminar steady-state flow near Re = 100 to turbulent flow at $Re=10^6$. Two different turbulence modeling approaches i.e. RANS based BSLRSM and LES are adopted. The comparison between the computed and available results of drag coefficients at different Reynolds numbers is shown in Figures 4.1 (a) and (b).

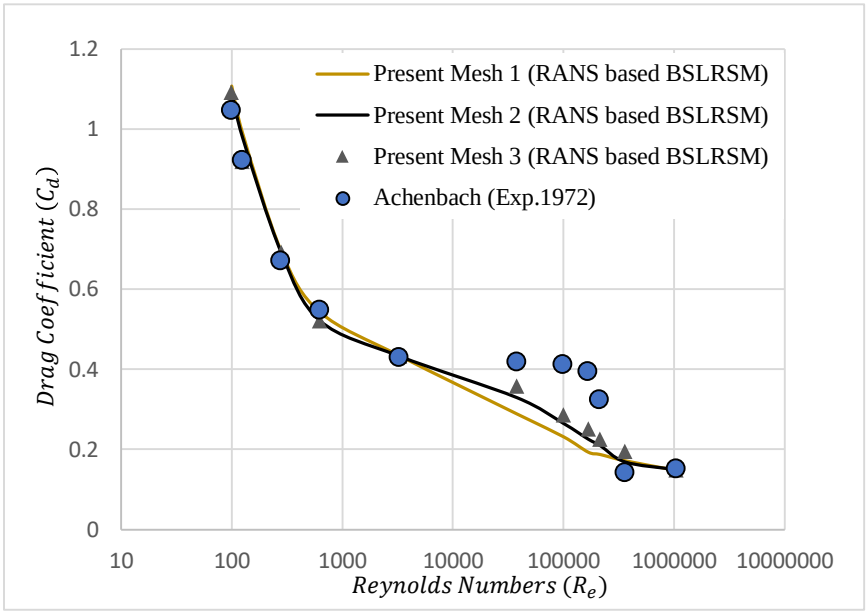

(a)

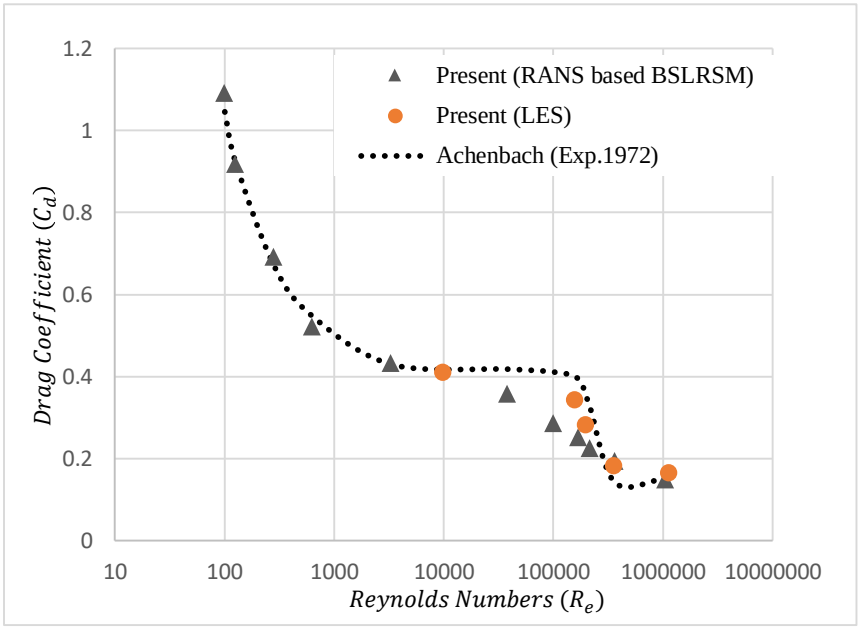

(b)

Figure 4.1. Comparison between the calculated values of drag coefficient with the experimental results

It can be observed that, in the laminar flow regime ($Re \leq 10^4$), the simulated results in both cases are in close agreement with experimental data. However, for higher Reynolds number ($Re > 10^4$), wakes flow becomes turbulent, values of drag coefficient calculated using LES are closer to experimental data as compared to those calculated using RANS based turbulence model. Furthermore, as $Re \geq 5 \times 10^5$, flow is become fully turbulent and calculated values using both approaches convergence towards experiments data.

The time-history of the drag coefficient at $R_E = 1.4 \times 10^5$ is presented in Figure 4.2. The fluctuations in the flow is due to vortex shedding. The mean C_d is 0.348.

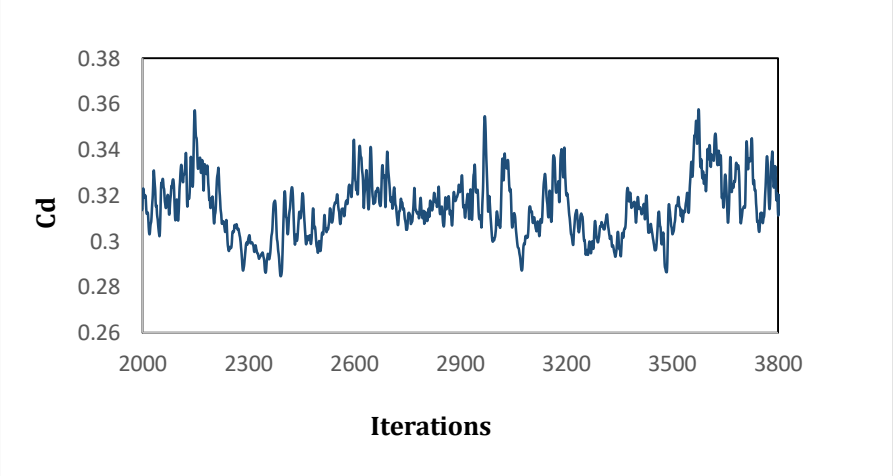

Figure. 4.2. Time-history of the drag coefficient

The pressure distribution around the smooth sphere in the three different flow regimes i.e. sub-critical and critical and supercritical flow regime are plotted in Figures 4.3 (a), (b) and (c) respectively. The corresponding Reynolds number are $Re = 1 \times 10^4$, $Re = 3.18 \times 10^5$ and $Re = 1.41 \times 10^6$, respectively. The polar angle φ is measured from the front stagnation point. The calculated results are compared with Achenbach's experimental and M. Muto's numerical data values.

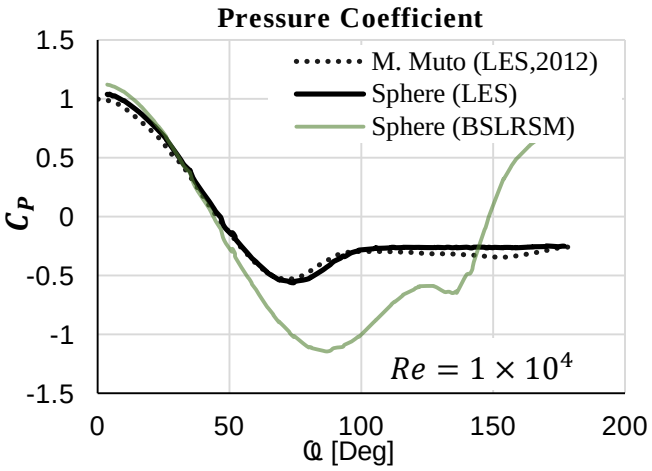
Pressure Coefficient
M. Muto (LES,2012)
Sphere (LES)
Sphere (BSLRSM)
C_P
$Re = 1 \times 10^4$
1.5
1
0.5
0
-0.5
-1
-1.5
0
50
100
150
200
Ø [Deg]

(a)

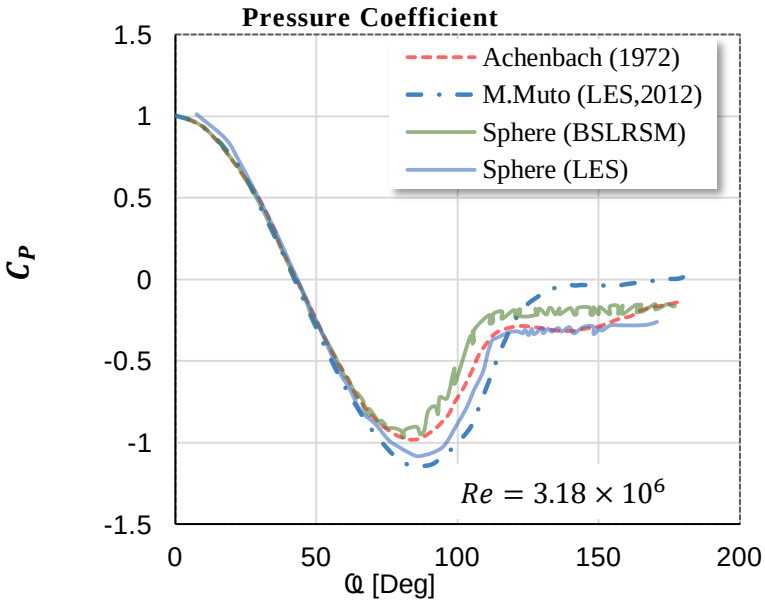
Pressure Coefficient
Achenbach (1972)
M.Muto (LES,2012)
Sphere (BSLRSM)
Sphere (LES)
C_P
$Re = 3.18 \times 10^6$
1.5
1
0.5
0
-0.5
-1
-1.5
0
50
100
150
200
Ø [Deg]

(b)

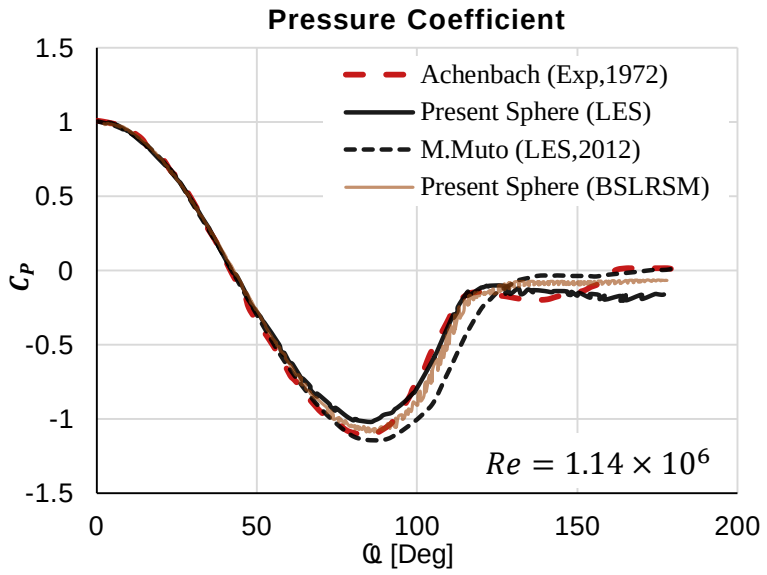

(c)

Figure 4.3. Surface pressure distributions (a)$\boldsymbol{Re = 1 \times 10^4}$, (b) $\boldsymbol{Re = 3.18 \times 10^5}$, and (c) $\boldsymbol{Re = 1.41 \times 10^6}$

It can be observed that from the Figures 4.3. (a)-(c), that the calculated results are in the close agreement with the available results. A significant drop in the pressure profile due to the transition from laminar to turbulent boundary layer can be observed in the critical flow regime. This also results in the delay of flow separation.

Figure 4.4 show the contours of the instantaneous stream wise velocity (x-component) at the three Reynolds numbers under consideration. It is also evident from these figures that as the Reynolds number increases, the separation angle increases and width of the wake region behind sphere became narrower.

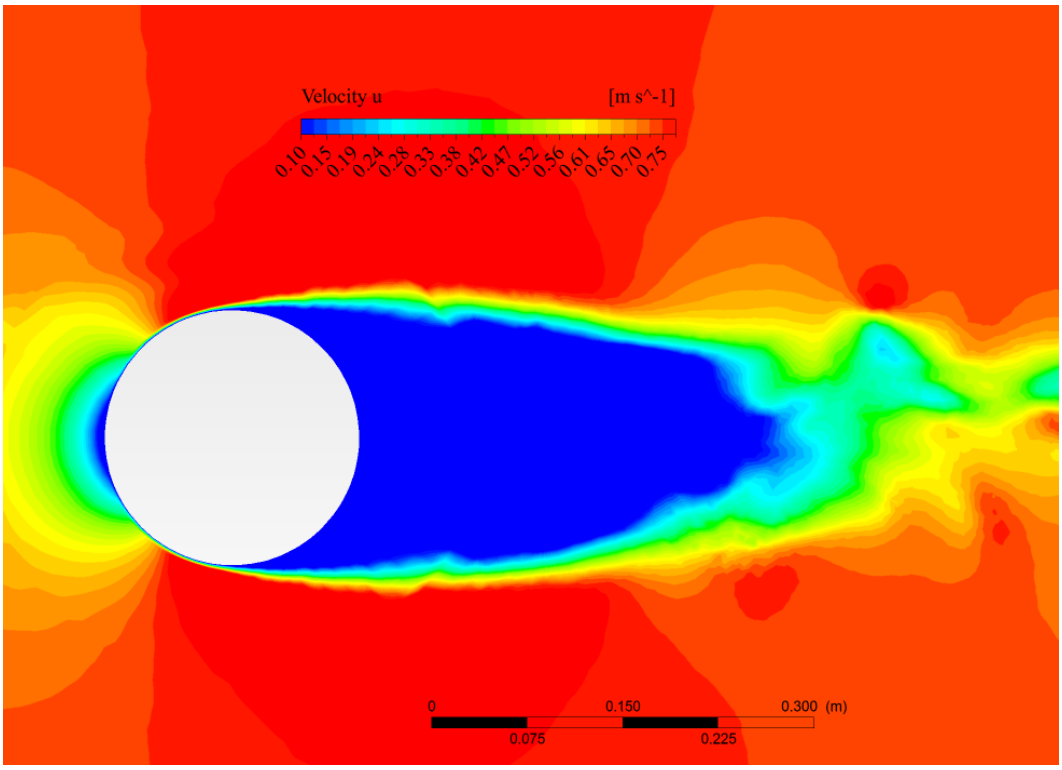
Velocity u
[m s^-1]
0.10
0.15
0.19
0.24
0.28
0.33
0.38
0.42
0.47
0.52
0.56
0.61
0.65
0.70
0.75
0
0.150
0.300 (m)
0.075
0.225

(a)

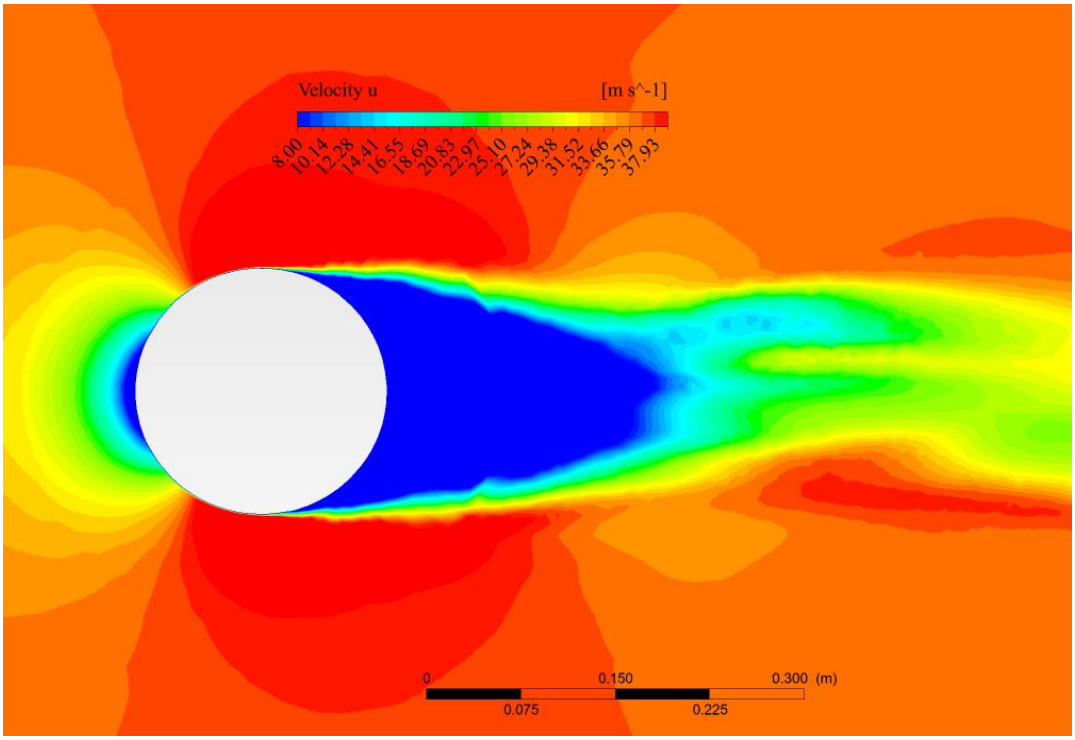
Velocity u
[m s^-1]
8.00
10.14
12.28
14.41
16.55
18.69
20.83
22.97
25.10
27.24
29.38
31.52
33.66
35.79
37.93
0
0.150
0.300 (m)
0.075
0.225

(b)

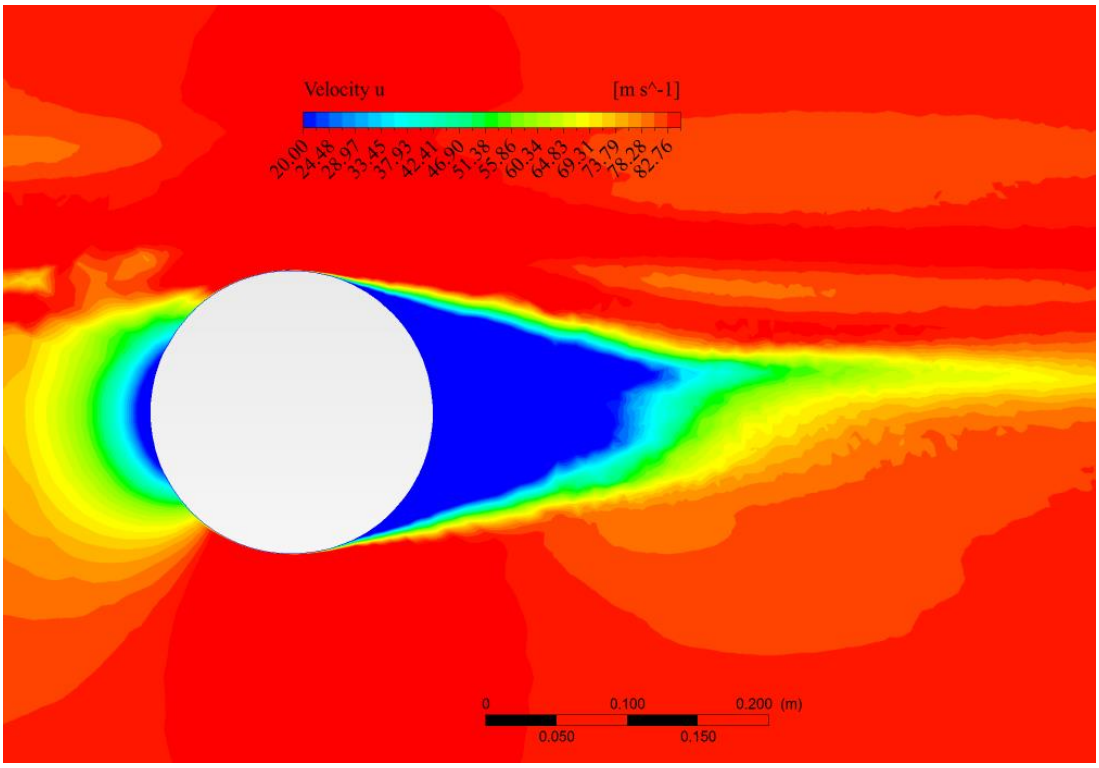

(c)

Figure 4.4. Contours of instantaneous x-component of velocity on central cross-section around sphere (a) $\boldsymbol{Re = 1 \times 10^4}$, (b) $\boldsymbol{Re = 3.18 \times 10^5}$, and (c) $\boldsymbol{Re = 1.41 \times 10^6}$

So it can be concluded that LES is preferable turbulence modeling approach while simulating the flow around a sphere especially in the critical flow regime. The same turbulence modeling approach is used in the second phase of the study i.e. while analyzing the effect of the panel shape on the soccer ball aerodynamics.

4.2 Flow Simulation around Soccer balls

In the second phase of the project, the flow around the two different soccer balls i.e. Adidas Brazuca and Telstar 18 are simulated using LES. The meshing strategy, boundary conditions and solution techniques validated in the first phase of the study are employed.

Soccer ball is mostly played in the wind speed range 7m/s to 35m/s. This corresponds to the speed range of 16 mph to78 mph and a Reynolds number range of $10^5 < \mathrm{Re} < 5 \times 10^5$[57].

So, the simulations are performed at the different incoming flow velocities ranging from 7m/s to 35m/s.

Figure 4.5 shows the comparison of simulated results of drag coefficients of the two soccer balls with experimental data. It can be observed that both Brazuca and Telstar 18 have approximately the same critical speed. Telstar 18 has a smaller drag coefficient than that of Brazuca in the narrow speed range. Though, Telstar 18 mostly has slightly larger drag coefficients.

However, the drag coefficient values in both cases are slightly over predicted. This difference between the simulated and experimental results can be due to the following reasons

1. The original Brazuca and telstar18 soccer balls have surface grooves which adds a layer of roughness. However, both soccer ball considered in the present study does not have any surface groove.
2. The panel orientation can have a significant effect on the aerodynamics of soccer balls [22]. The panel orientation during the current numerical study of the both soccer balls was not same as that of experiment.
3. The effects of the flow interaction between the soccer ball and its supporting device used in wind tunnel could not be taken into consideration.

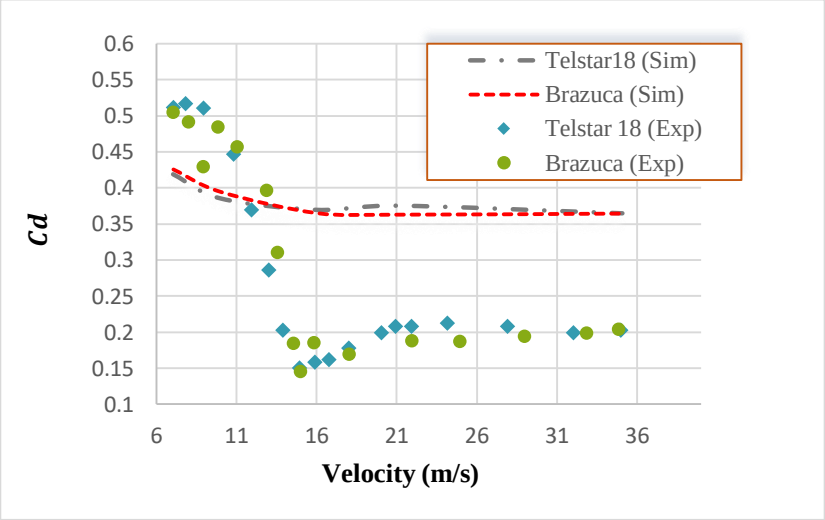

Figure 4.5. Drag coefficient as a function of velocity

The comparison between the pressure distributions on the surface of the soccer balls with that of sphere is shown in Figure 4.6. The C_p value of the soccer balls show some local fluctuation at several angular positions (as expected). Such variations are mainly affected by the panel distributed on the surface of the soccer balls. In case of Brazuca, he boundary layer separation take place around 98°, however, in case of Telstar-18 the separation angle is around 101°.

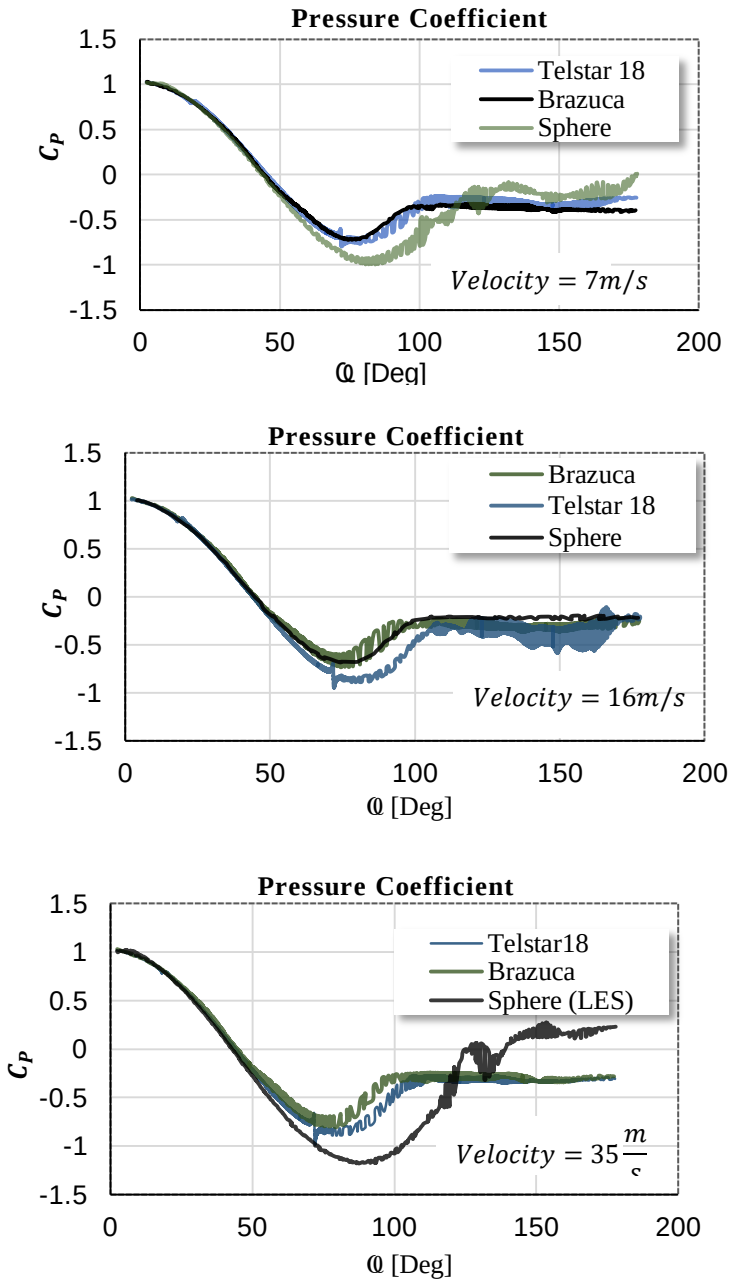

Figure 4.6. Surface pressure distribution

The shear stress distributions on the soccer balls' surface reveal the effect of seam and panels. It can be observed in the Figure 4.7. That wall shear stress changes locally in regions near the seams due to the localized small flow structures. Figure 4.8 show the velocity streamlines around both soccer balls.

Figure 4.9 show the wake behind the Brazuca and Telstar-18vortex. It can be observed that flow remain toTelstar18 a little longer than Brazuca. Similarly, the Brazuca has a wider wake as compared to Telstar 18.

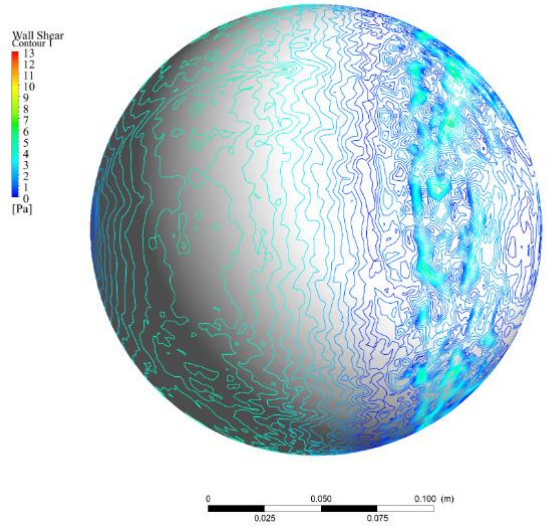

(a)

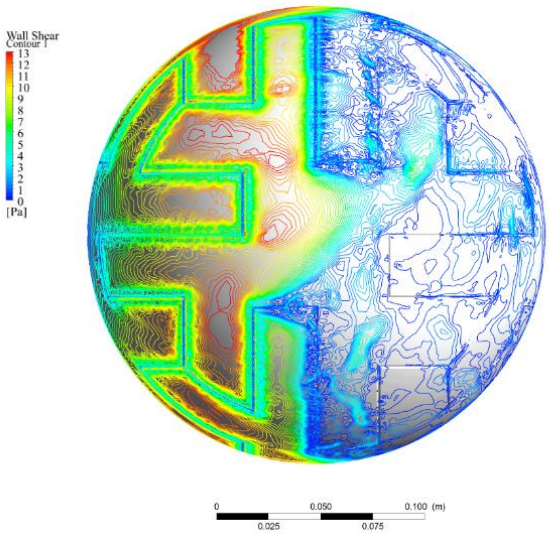

(b)

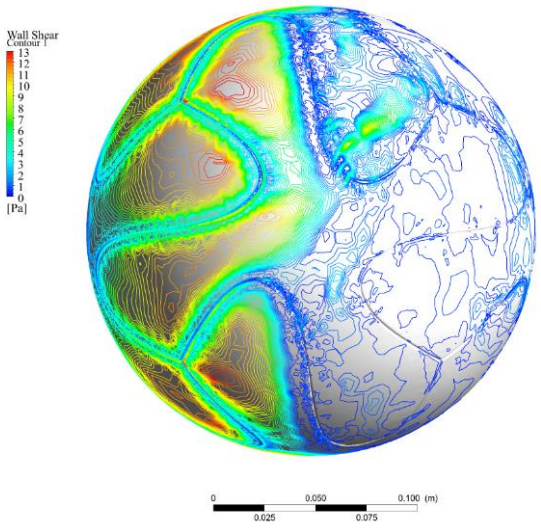

(c)

Figure. 4.7. The surface shear stress distributions for (a) Smooth Sphere, (b) Addidas Telstar 18, and (c) Brazuca

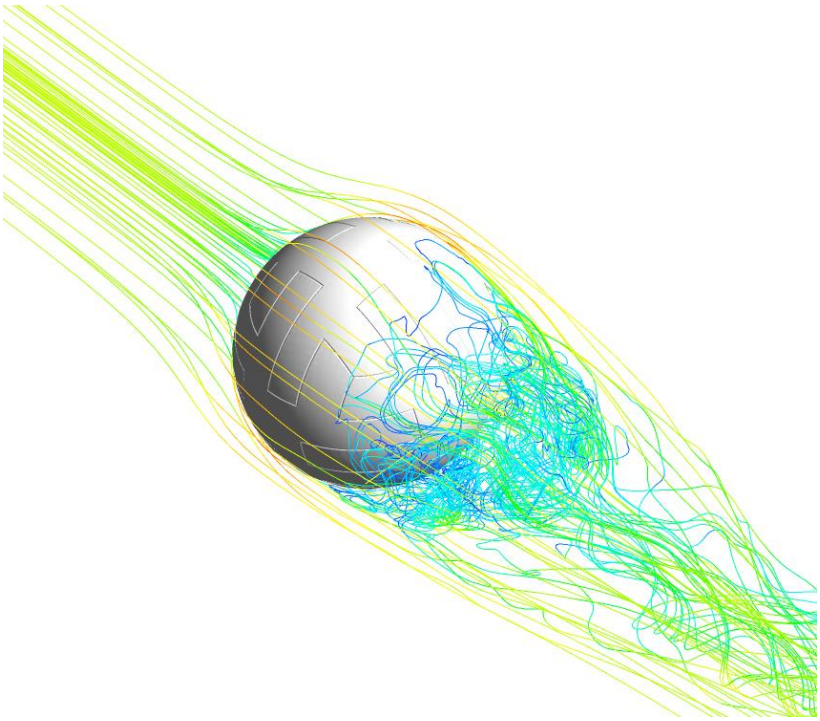

(a)

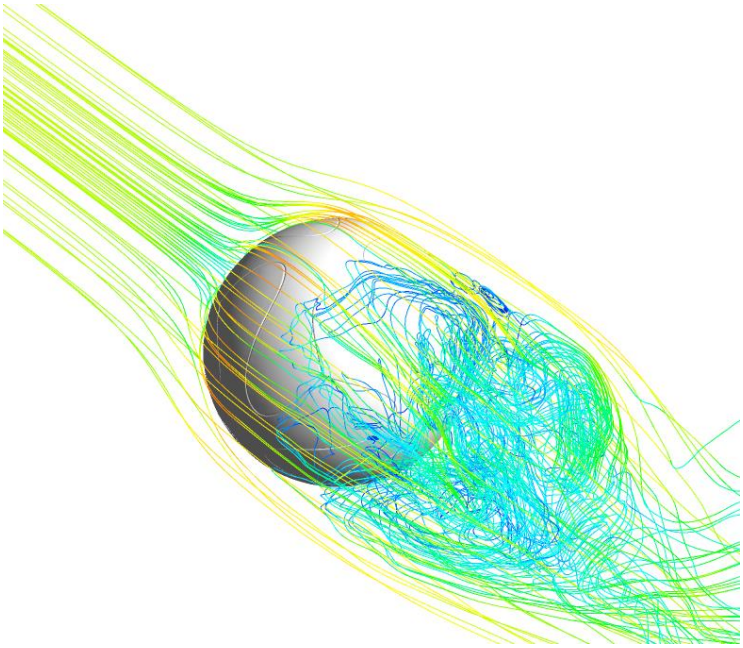

(b)

Figure. 4.8. Velocity streamlines around (a) Addidas Telstar 18, and (b) Brazuca

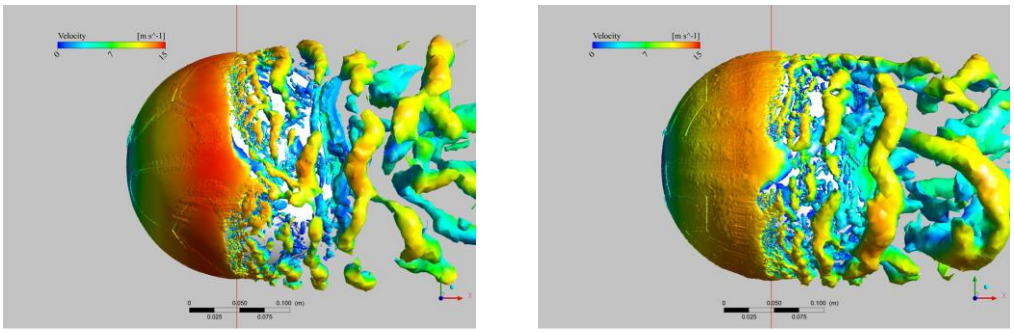

Vortex core region on soccer balls at Velocity = 10 m/s

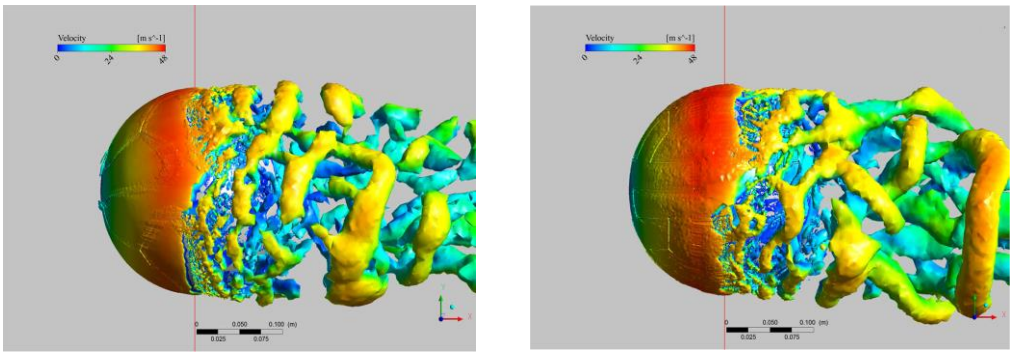

Vortex core region on soccer balls at Velocity = 35 m/s

Figure 4.9. Visualization of unsteady wake

CHAPTER 5: CONCLUSIONS AND FUTURE SCOPE OF WORK

A brief summary of conclusive results derived from the current research is given in this chapter. Some recommendations for future efforts in this area are also suggested.

5.1 Conclusions

The aim of this research is to understand the effect of panel shape on soccer ball aerodynamics using computational fluid dynamics techniques. The main conclusions pinched from the above research are following:

1. RANS based turbulence modeling approach can be used for simulating the flow around a sphere in the laminar flow regime ($Re \leq 10^4$)
2. However, for higher Reynolds number ($Re > 10^4$), wakes flow becomes turbulent and flow simulation using LES is a more appropriate choice.
3. A significant drop in the pressure profile around the sphere surface is observed in the critical flow regime. This is due to the transition from laminar to turbulent boundary layer which also results in the delay of flow separation.
4. Both Brazuca and Telstar 18 have approximately the same critical speed. Telstar 18 has a smaller drag coefficient than that of Brazuca in the narrow speed range. Nevertheless, Telstar 18 mostly has slightly larger drag coefficients.
5. The C_p values of the soccer balls show some local fluctuation at several angular positions (as expected). Such variations are mainly affected by the panel distributed on the surface of the soccer balls.
6. In case of Brazuca, he boundary layer separation take place around 98^o, however, in case of Telstar-18 the separation angle is around 101^o.
7. The surface shear stress changes locally in regions near the seams due to the localized small flow structures.
8. It can be concluded that the effect of the panel shape is more significant on the flow around the soccer balls as compared to soccer ball drag.

5.2 Future Scope of Work

Following are the main suggestions for the future work in the area of soccer ball aerodynamics

1. The effect of panel orientation on the soccer ball aerodynamics needs to be evaluated numerically.
2. The effect of the panel shape on the aerodynamics and flight trajectory of the spinning soccer balls needs to be investigated.

References

1. https://www.kreedon.com/fifa-world-cup-soccer-balls/.
2. Naito, K., Hong, S., Koido, M., Nakayama, M., Sakamoto, K. and Asai, T., 2018. Effect of seam characteristics on critical Reynolds number in footballs. *Mechanical Engineering Journal*, *5*(1), pp.17-00369.
3. Hong, S. and Asai, T., 2014. Effect of panel shape of soccer ball on its flight characteristics. *Scientific reports*, *4*, p.5068.
4. Goff, J.E., Hong, S. and Asai, T., 2020. Influence of Surface Properties on Soccer Ball Trajectories. In *Multidisciplinary Digital Publishing Institute Proceedings* (Vol. 49, No. 1, p. 143).
5. Barber, S. and Carré, M.J., 2010. The effect of surface geometry on soccer ball trajectories. Sports Engineering, 13(1), pp.47-55.
6. Alam, F., Chowdhury, H., Stemmer, M., Wang, Z. and Yang, J., 2012. Effects of surface structure on soccer ball aerodynamics. *Procedia Engineering*, *34*, pp.146-151.
7. Hong, S., Goff, J.E. and Asai, T., 2019. Effect of a soccer ball's surface texture on its aerodynamics and trajectory. *Proceedings of the Institution of Mechanical Engineers, Part P: Journal of Sports Engineering and Technology*, *233*(1), pp.67-74.
8. Goff, J.E., Asai, T. and Hong, S., 2014. A comparison of Jabulani and Brazuca non-spin aerodynamics. *Proceedings of the Institution of Mechanical Engineers, Part P: Journal of Sports Engineering and Technology*, *228*(3), pp.188-194.
9. Zafar, F., Nawaz, I., Aqib, M., Shahzad, N. and Yasir, M., 2017. Contribution of Sports Goods Industry towards Economic Growth of Pakistan. *Advances in Social Sciences Research Journal*, *4*(13), pp.70-75
10. Carré, M.J., Goodwill, S.R. and Haake, S.J., 2005. Understanding the effect of seams on the aerodynamics of an association football. *Proceedings of the Institution of Mechanical Engineers, part C: Journal of mechanical engineering science*, *219*(7), pp.657-666.

11. Asai, T., Seo, K., Kobayashi, O. and Sakashita, R., 2006. Flow visualization on a real flight non-spinning and spinning soccer ball. In *The Engineering of Sport 6* (pp. 327-332). Springer, New York, NY.
12. Asai, T., Seo, K., Kobayashi, O. and Sakashita, R., 2007. Fundamental aerodynamics of the soccer ball. *Sports Engineering*, *10*(2), pp.101-109.
13. Oggiano, L. and Sætran, L., 2010. Aerodynamics of modern soccer balls. *Procedia Eng*, *2*(2), pp.2473-2479.
14. Passmore, M., Rogers, D., Tuplin, S., Harland, A., Lucas, T. and Holmes, C., 2012. The aerodynamic performance of a range of FIFA-approved footballs. *Proceedings of the Institution of Mechanical Engineers, Part P: Journal of Sports Engineering and Technology*, *226*(1), pp.61-70.
15. Asai, T., Ito, S., Seo, K. and Koike, S., 2012. Characteristics of modern soccer balls. *Procedia Engineering*, *34*, pp.122-127.
16. Asai, T. and Seo, K., 2013. Aerodynamic drag of modern soccerballs. *SpringerPlus*, *2*(1), p.171.
17. Alam, F., Chowdhury, H., Moria, H. and Fuss, F.K., 2010. A comparative study of football aerodynamics. *Procedia Engineering*, *2*(2), pp.2443-2448.
18. Alam, F., Chowdhury, H., Moria, H., Fuss, F.K., Khan, I., Aldawi, F. and Subic, A., 2011. Aerodynamics of contemporary FIFA soccer balls. *Procedia Engineering*, *13*, pp.188-193.
19. Alam, F., Chowdhury, H., George, S., Mustary, I. and Zimmer, G., 2014. Aerodynamic drag measurements of FIFA-approved footballs. *Procedia Engineering*, *72*, pp.703-708.
20. Alam, F., Chowdhury, H., Loganathan, B., Mustary, I. and Watkins, S., 2014, December. Aerodynamic Drag of Contemporary Soccer Balls. In *19th Australasian Proceedings of Fluid Mechanics Conference, Melbourne, Australia*.
21. Hong, S., Sakamoto, K., Washida, Y., Nakayama, M. and Asai, T., 2014. The influence of panel orientation on the aerodynamics of soccer balls. *Procedia Engineering*, *72*, pp.786-791.
22. Hong, S. and Asai, T., 2017. Aerodynamic effects of dimples on soccer ball surfaces. *Heliyon*, *3*(10), p.e00432.

23. Carré, M.J., Goodwill, S.R. and Haake, S., 2004. Understanding the aerodynamics of a spinning soccer ball. In *The 5th international conference on the engineering of sport* (Vol. 1, pp. 70-76). International sports engineering assocation.
24. Barber, S., Haake, S.J. and Carré, M., 2006. Using CFD to understand the effects of seam geometry on soccer ball aerodynamics. In *The Engineering of Sport 6* (pp. 127-132). Springer, New York, NY.
25. Barber, S., Chin, S.B. and Carré, M.J., 2009. Sports ball aerodynamics: a numerical study of the erratic motion of soccer balls. *Computers & Fluids*, *38*(6), pp.1091-1100.
26. Jalilian, P., Kreun, P.K., Makhmalbaf, M.M. and Liou, W.W., 2014. Computational aerodynamics of baseball, soccer ball and volleyball. *American Journal of Sports Science*, *2*(5), pp.115-121.
27. Rohr, A., 2018. *A Computational Fluid Dynamics (Cfd) Analysis of the Aerodynamic Effects of the Seams on a Two-Dimensional Representation of a Soccer Ball* (Doctoral dissertation, California Polytechnic State University, San Luis Obispo).
28. Hussain, S.B., Shah, S.I.A. and Shahzad, A., 2020, February. Optimization and Aerodynamic Design of a Soccer Ball Using Numerical Analysis. In *2020 International Conference on Engineering and Emerging Technologies (ICEET)* (pp. 1-7). IEEE.
29. Asai, T., Nakanishi, Y., Akiyama, N. and Hong, S., 2020. Flow Visualization of Spinning and Nonspinning Soccer Balls Using Computational Fluid Dynamics. *Applied Sciences*, *10*(13), p.4543.
30. Bray, K. and Kerwin, D., 2003. Modelling the flight of a soccer ball in a direct free kick. Journal of sports sciences, 21(2), pp.75-85.
31. Goff, J.E. and Carré, M.J., 2009. Trajectory analysis of a soccer ball. *American Journal of Physics*, *77*(11), pp.1020-1027
32. Goff, J.E. and Carré, M.J., 2012. Investigations into soccer aerodynamics via trajectory analysis and dust experiments. *Procedia Engineering*, *34*, pp.158-163.
33. Goff, J.E., Kelley, J., Hobson, C.M., Seo, K., Asai, T. and Choppin, S.B., 2017. Creating drag and lift curves from soccer trajectories. *European Journal of Physics*, *38*(4), p.044003.
34. Choppin, S., 2013. Calculating football drag profiles from simulated trajectories. *Sports Engineering*, *16*(3), pp.189-194.

35. Rogers, D., Passmore, M., Harland, A., Jones, R., Holmes, C. and Lucas, T., 2010. An experimental validation method of wind tunnel measurements on FIFA approved footballs using kicking tests in wind-free conditions. *Procedia Engineering*, *2*(2), pp.2481-2486.
36. Myers, T.G. and Mitchell, S.L., 2013. A mathematical analysis of the motion of an in-flight soccer ball. *Sports engineering*, *16*(1), pp.29-41.
37. Goff, J.E., Smith, W.H. and Carré, M.J., 2011. Football boundary-layer separation via dust experiments. *Sports Engineering*, *14*(2-4), pp.139-146.
38. Cook, B.G. and Goff, J.E., 2006. Parameter space for successful soccer kicks. *European journal of physics*, *27*(4), p.865.
39. Versteeg, H.K. and Malalasekera, W., 2007. *An introduction to computational fluid dynamics: the finite volume method*. Pearson education.
40. Härtel, C., 1996. Turbulent flows: direct numerical simulation and large-eddy simulation. In *Handbook of Computational Fluid Mechanics* (pp. 283-338). Academic Press.
41. Moin, P. and Mahesh, K., 1998. Direct numerical simulation: a tool in turbulence research. *Annual review of fluid mechanics*, *30*(1), pp.539-578.
42. Fox, D.G. and Lilly, D.K., 1972. Numerical simulation of turbulent flows. *Reviews of Geophysics*, *10*(1), pp.51-72.
43. Zhiyin, Y., 2015. Large-eddy simulation: Past, present and the future. *Chinese journal of Aeronautics*, *28*(1), pp.11-24.
44. Boris, J.P., Grinstein, F.F., Oran, E.S. and Kolbe, R.L., 1992. New insights into large eddy simulation. *Fluid dynamics research*, *10*(4-6), p.199.
45. Rao, J.S., 2017. *Simulation based engineering in fluid flow design*. Springer.
46. Pletcher, R.H., Tannehill, J.C. and Anderson, D., 2012. *Computational fluid mechanics and heat transfer*. CRC press, pp.249-285
47. Baldwin, B.S. and Lomax, H., 'Thin Layer Approximation and Algebraic Model for Separated Turbulent Flows,' AIAA Paper 78-0257, Jan. 1978.
48. Bardina, J.E., Huang, P.G. and Coakley, T.J., 1997. Turbulence modeling validation, testing, and development., NASA Ames Research Center; Moffett Field, CA United States
49. Craft, T.J., Launder, B.E. and Suga, K., 1996. Development and application of a cubic eddy-viscosity model of turbulence. *International Journal of Heat and Fluid Flow*, *17*(2), pp.108-115.

50. Leong, Z.Q., Ranmuthugala, D., Penesis, I. and Nguyen, H.D., 2012. Numerical simulation of spheres in relative motion using dynamic meshing techniques. In *18th Australasian Fluid Mechanics Conference* (pp. 1-4).
51. Schlichting, H., 1979. Boundary Layer Theory, McGraw-Hill, New York. pp.10
52. Jones, D.A. and Clarke, D.B., 2008. *Simulation of flow past a sphere using the fluent code.* Defense Science and Technology Organization Victoria (Australia) Maritime Platforms Div., Australia
53. Goff, J.E., Hong, S. and Asai, T., 2018. Aerodynamic and surface comparisons between Telstar 18 and Brazuca. *Proceedings of the Institution of Mechanical Engineers, Part P: Journal of Sports Engineering and Technology*, *232*(4), pp.342-348.
54. Achenbach, E., 1972. Experiments on the flow past spheres at very high Reynolds numbers. *Journal of Fluid Mechanics*, *54*(3), pp.565-575.
55. Muto, M., Tsubokura, M. and Oshima, N., 2012. Negative Magnus lift on a rotating sphere at around the critical Reynolds number. *Physics of Fluids*, *24*(1), p.014102.